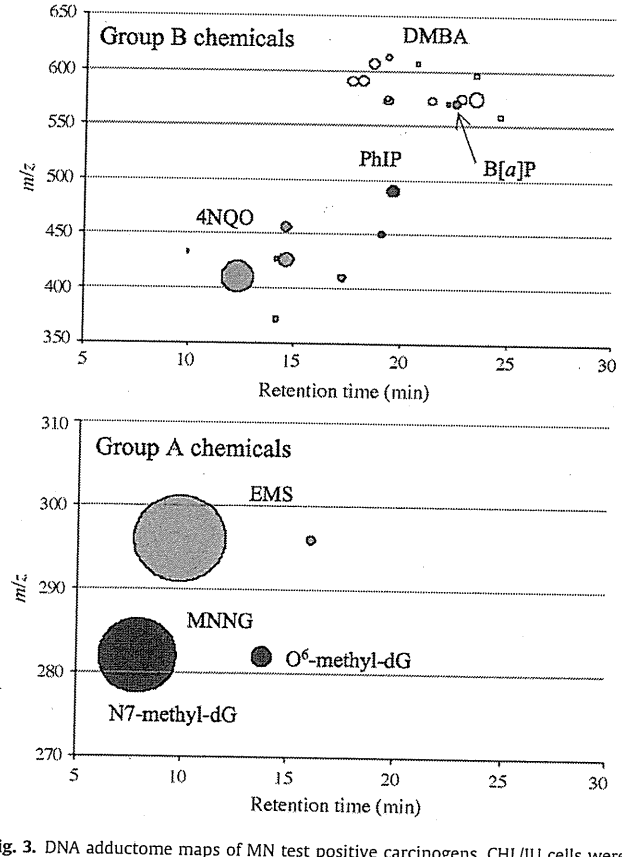

Fig. 3. DNA adductome maps of MN test positive carcinogens. CHL/IU cells were treated with Group A chemicals (carcinogens causing DNA alkylation) or Group B chemicals (carcinogens producing bulky DNA adducts), and the extracted DNA was digested by the MCN/SPD method (MNNG, EMS, B[*a*]P, DMBA) or nuclease P1 method (4-NQO and PhIP). The size of each bubble represents the "normalized peak area" shown in Table 2. Group A chemicals: EMS, pink; MNNG, brown. Group B chemicals: PhIP, blue; B[*a*]P, red; DMBA, yellow; 4-NQO, green. (For interpretation of the references to colour in this figure legend, the reader is referred to the web version of this article.)

sively, (2) the structures of the detected adducts can be identified from their *m/z* and their analytical standards, and (3) various experimental designs can be applied to both *in vitro* and *in vivo* samples. These experimental features resolve some limitations of the existing methods for analyzing DNA adduct formation.

This study is a pilot experiment to confirm the usefulness of the adductome approach to detect DNA adduct s produced by the compounds showing positive results in the MN test with different MOA. This approach enables detection of various types of DNA adducts formed by typical carcinogens, and does not enable detection of any adducts for non-carcinogens. We conclude that the adductome approach would be applicable to assess the DNA-damaging capability of many types of *in vitro* MN test-positive compounds, and also be useful for understanding MOA of the test compounds.

Conflicts of interest

The authors have no conflicts of interest to declare.

Acknowledgements

This research was performed as a cooperative research project among three institutions, Mitsubishi Tanabe Pharma Corporation, Kyoto University, and Osaka Prefecture University, which was supported by a fund from Mitsubishi Tanabe Pharma Corporation.

Appendix A. Supplementary data

Supplementary data associated with this article can be found, in the online version, at doi:10.1016/j.mrgentox.2010.11.012.

References

[1] D. Kirkland, M. Aardema, L. Henderson, L. Müller, Evaluation of the ability of a battery of 3 *in vitro* genotoxicity tests to descriminate rodent carcinogens and non-carcinogens. I. Sensitivity, specificity and relative predictivity, Mutat. Res. 584 (2005) 1–256.
[2] G.M. Williams, J. Whysner, Epigenetic carcinogens: evaluation and risk assessment, Exp. Toxicol. Pathol. 48 (1996) 189–195.
[3] D.H. Phillips, P.B. Farmer, F.A. Beland, R.G. Nath, M.C. Poirier, M.V. Reddy, K.W. Turteltaub, Methods of DNA adduct determination and their application to testing compounds for genotoxicity, Environ. Mol. Mutagen. 25 (2000) 222–233.
[4] R.A. Kanaly, T. Hanaoka, H. Sugimura, H. Toda, S. Matsui, T. Matsuda, Development of the adductome approach to detect DNA damage in humans, Antioxid. Redox Signal. 8 (2006) 993–1001.
[5] Y. Yang, D. Mikolic, S.M. Swanson, R.B. van Breeman, Quantitative determination of N^7-methyldeoxyguanosine and O^6-methyldeoxyguanosine in DNA by LC–UV–MS–MS, Anal. Chem. 74 (2002) 5376–5382.
[6] D.T. Beranek, Distribution of methyl and ethyl adducts following alkylation with monofunctional alkylating agents, Mutat. Res. 231 (1990) 11–30.
[7] P.D. Lowley, C.J. Thatcher, Methylation of deoxyribonucleic acid in cultured mammalian cells by *N*-methyl-*N'*-nitro-*N*-nitrosoguanidine, Biochem. J. 116 (1970) 693–707.
[8] D. Lin, K.R. Kaderlik, R.J. Turesky, D.W. Miller, J.O. Lay Jr., F.F. Kadlubar, Identification of *N*-(deoxyguanosin-8-yl)-2-amino-1-methyl-6-phenylimidazo[4,5-b]pyridine as the major adduct Formed by the food-borne carcinogen, 2-amino-1-methyl-6-phenylimidazo[4,5-b]pyridine, with DNA, Chem. Res. Toxicol. 5 (1992) 691–697.
[9] Q. Ruan, H.H. Kim, H. Jiang, T.M. Penning, R.G. Harvey, I.A. Blair, Quantification of benzo[a]pyrene diol epoxide DNA-adducts by stable isotope dilution liquid chromatography/tandem mass spectrometry, Rapid Commun. Mass Spectrom. 20 (2006) 1369–1380.
[11] K.W. Singletary, H.M. Parker, J.A. Milner, Identification and *in vivo* formation of ^{32}P-postlabeled rat mammary DMBA-DNA adducts, Carcinogenesis 11 (1990) 1959–1963.
[12] S. Galiègue-Zoutina, B. Bailleul, M. Loucheux-Lefevre, Adducts from *in vivo* auction of the carcinogen 4-hydroxyaminoquinoline 1-oxide in rats and from *in vitro* reaction of 4-acetoxyaminoquinoline 1-oxide with DNA and polynucleotides, Cancer Res. 45 (1985) 520–525.
[13] B. Bailleul, S. Galiègue, M. Loucheux-Lefebre, Adducts from the Reaction of O, O'-diacetyl or o-acetyl derivatives of the carcinogen 4-hydroxyaminoquinoline 1-oxide with purine nucleosides, Cancer Res. 41 (1981) 4559–4565.
[14] B. Bailleul, S. Galiègue-Zoutina, B. Perly, M. Loucheux-Lefebre, Structural identification of the purine ring-opened form of *N*-(deoxyguanosine-8yl)-4-aminoquinoline 1-oxide, Carcinogenesis 6 (1985) 319–332.
[15] S. Galiègue-Zoutina, B. Bailleul, Y. Ginot, B. Perly, P. Vigny, M. Loucheux-Lefebre, N^2-guanyl and N^6-adenyl arylation of chicken erythrocyte DNA by the ultimate carcinogen of 4-nitroquinoline 1-oxide, Cancer Res. 46 (1986) 1858–1863.
[16] Y. Arima, C. Nishigori, T. Takeuchi, S. Oka, K. Morimoto, A. Utani, Y. Miyachi, 4-nitroquinoline 1-oxide forms 8-hydroxydeoxyguanosine in human fibroblasts through reactive oxygen species, Toxicol. Sci. 91 (2006) 382–392.
[17] T. Hofer, C. Badouard, E. Bajak, J. Ravanat, Å. Mattsson, I.A. Cotgreave, Hydrogen peroxide causes greater oxidation in cellular RNA than DNA, Biol. Chem. 386 (1995) 333–337.
[18] H.S. Rosenkranz, F.K. Ennever, Evaluation of the genotoxicity of theobromine and caffeine, Food Chem. Toxicol. 25 (1987) 247–251.
[19] W.U. Müller, T. Bauch, A. Wojcik, W. Böcker, C. Streffer, Comet assay studies indicate that caffeine-mediated increase in radiation risk of embryos is due to inhibition of DNA repair, Mutagenesis 11 (1996) 57–60.
[20] K. Murakami, K. Ishida, K. Watanabe, R. Tsubouchi, M. Haneda, M. Yoshino, Prooxidant action of maltol: role of transition metals in the generation of reactive oxygen species and enhanced formation of 8-hydroxy-2'-deoxyguanosine formation in DNA, Biometals 19 (2006) 253–257.
[21] S.M. Galloway, D.A. Deasy, C.L. Bean, A.R. Kraynak, M.J. Armstrong, M.O. Bradley, Effects of high osmotic strength on chromosome aberrations, sister-chromatid exchanges and DNA strand breaks, and the relation to toxicity, Mutat. Res. 189 (1987) 15–25.

Chem. Res. Toxicol. **2010,** *23,* 1442–1448

Detection of Lipid Peroxidation-Induced DNA Adducts Caused by 4-Oxo-2(*E*)-nonenal and 4-Oxo-2(*E*)-hexenal in Human Autopsy Tissues

Pei-Hsin Chou,[†,‡] Shinji Kageyama,[§] Shun Matsuda,[†] Keishi Kanemoto,[†] Yoshiaki Sasada,[†] Megumi Oka,[†] Kazuya Shinmura,[§] Hiroki Mori,[§] Kazuaki Kawai,[∥] Hiroshi Kasai,[∥] Haruhiko Sugimura,*[,§] and Tomonari Matsuda*[,†]

Research Center for Environmental Quality Management, Kyoto University, Otsu, Shiga, 520-0811, Japan, Department of Environmental Engineering, National Cheng Kung University, Tainan, 70101, Taiwan, Department of Pathology, Hamamatsu University School of Medicine, Hamamatsu, Shizuoka, 431-3192, Japan, and Department of Environmental Oncology, University of Occupational and Environmental Health, Kitakyushu, Fukuoka, 807-8555, Japan

Received February 8, 2010

DNA adducts are produced both exogenously and endogenously via exposure to various DNA-damaging agents. Two lipid peroxidation (LPO) products, 4-oxo-2(*E*)-nonenal (4-ONE) and 4-oxo-2(*E*)-hexenal (4-OHE), induce substituted etheno-DNA adducts in cells and chemically treated animals, but the adduct levels in humans have never been reported. It is important to investigate the occurrence of 4-ONE- and 4-OHE-derived DNA adducts in humans to further understand their potential impact on human health. In this study, we conducted DNA adductome analysis of several human specimens of pulmonary DNA as well as various LPO-induced DNA adducts in 68 human autopsy tissues, including colon, heart, kidney, liver, lung, pancreas, small intestine, and spleen, by liquid chromatography tandem mass spectrometry. In the adductome analysis, DNA adducts derived from 4-ONE and 4-OHE, namely, heptanone-etheno-2′-deoxycytidine (HεdC), heptanone-etheno-2′-deoxyadenosine (HεdA), and butanone-etheno-2′-deoxycytidine (BεdC), were identified as major adducts in one human pulmonary DNA. Quantitative analysis revealed 4-ONE-derived HεdC, HεdA, and heptanone-etheno-2′-deoxyguanosine (HεdG) to be ubiquitous in various human tissues at median values of 10, 15, and 8.6 adducts per 10^8 bases, respectively. More importantly, an extremely high level (more than 100 per 10^8 bases) of these DNA adducts was observed in several cases. The level of 4-OHE-derived BεdC was highly correlated with that of HεdC ($R^2 = 0.94$), although BεdC was present at about a 7-fold lower concentration than HεdC. These results suggest that 4-ONE- and 4-OHE-derived DNA adducts are likely to be significant DNA adducts in human tissues, with potential for deleterious effects on human health.

Introduction

Lipid peroxidation (LPO[1]) is a major source of DNA-damaging agents. Decomposition products generated from the LPO of polyunsaturated fatty acids (PUFAs) are highly DNA-reactive, including acrolein, crotonaldehyde, malondialdehyde, and other α,β-unsaturated aldehydes (*1–3*). These electrophilic aldehydes may modify nucleic acid bases to form DNA adducts implicated in mutagenesis, carcinogenesis, accelerated aging, or neurological deterioration (*4–6*). Thus, investigation into the levels and tissue distributions of LPO-derived DNA adducts in humans is important to further understand their possible impact on human health.

LPO-related DNA adducts identified in human tissues are mainly exocyclic etheno and propano adducts such as 1,N^6-etheno-2′-deoxyadenosine (εdA); 3,N^4-etheno-2′-deoxycytidine (εdC); 1, N^2-propano-2′-deoxyguanosines generated from acrolein, crotonaldehyde, and 4-hydroxy-2(*E*)-nonenal (4-HNE); and malondialdehyde-derived 3-(2-deoxy-β-D-erythro-pentofuranosyl)pyrimido[1,2-α]purin-10(3*H*)-one (*7–9*). The long-chain aldehyde 4-HNE is an ω-6 PUFA-peroxidation product that reacts with DNA and protein (*10–12*); furthermore, 4-HNE-related DNA adducts have been reported to be associated with carcinogenesis and Alzheimer's disease (*13–15*). 4-Oxo-2(*E*)-nonenal (4-ONE), another decomposition product of ω-6 PUFAs, has also been shown to induce the formation of etheno DNA adducts carrying aliphatic side chains both in cells and in mouse models, including heptanone-etheno-2′-deoxycytidine (HεdC), heptanone-etheno-2′-deoxyguanosine (HεdG), and heptanone-etheno-2′-deoxyadenosine (HεdA) (*16–18*). 4-Oxo-2(*E*)-hexenal (4-OHE), an ω-3 PUFA-peroxidation product having a chemical structure similar to that of 4-ONE, was recently reported to be able to produce etheno DNA adducts as well,

* Corresponding author. (H.S. (for medical questions)) E-mail: hsugimur@hama-med.ac.jp. (T.M. (for DNA adduct analysis)) E-mail: matsuda@z05.mbox.media.kyoto-u.ac.jp.

† Kyoto University.

‡ National Cheng Kung University.

§ Hamamatsu University School of Medicine.

∥ University of Occupational and Environmental Health.

[1] Abbreviations: PUFA, polyunsaturated fatty acid; LPO, lipid peroxidation; 4-HNE, 4-hydroxy-2(*E*)-nonenal; 4-ONE, 4-oxo-2(*E*)-nonenal; 4-OHE, 4-oxo-2(*E*)-hexenal; HεdC, heptanone-etheno-2′-deoxycytidine; HεdG, heptanone-etheno-2′-deoxyguanosine; HεdA, heptanone-etheno-2′-deoxyadenosine; BεdC, butanone-etheno-2′-deoxycytidine; BεmedC, butanone-etheno-2′-deoxy-5-methylcytidine; BεdG, butanone-etheno-2′-deoxyguanosine; BεdA, butanone-etheno-2′-deoxyadenosine; 8-oxodG, 8-oxo-7,8-dihydro-2′-deoxyguanosine; εdA, 1,N^6-etheno-2′-deoxyadenosine; 8-OH-AdG, 8-hydroxy-1,N^2-propanodeoxyguanosine; CdG_2, α-*R*-methyl-γ-hydroxy-1,N^2-propano-2′-deoxyguanosine;COX-2, cyclooxygenase-2; HPNE, 4-hydroperoxy-2(*E*)-nonenal; EDE, 4,5-epoxy-2(*E*)-decenal; 5-LO, 5-lipoxygenase.

10.1021/tx100047d
Published on Web 07/23/2010

such as butanone-etheno-2′-deoxycytidine (BεdC), butanone-etheno-2′-deoxy-5-methyl-cytidine (BεmedC), butanone-etheno-2′-deoxyguanosine (BεdG) (*19–21*), and butanone-etheno-2′-deoxyadenosine (BεdA) (*22*). The levels of 4-ONE- and 4-OHE-related DNA adducts in humans are currently unknown because such adducts were discovered only very recently.

In addition to LPO-derived DNA adducts, various other types of DNA lesions are frequently formed in humans as a consequence of exposure to environmental carcinogens or endogenous DNA-reactive agents. Because a variety of DNA adducts are present in human tissues, comprehensive investigation of these base modifications is necessary to identify the ones most critical to mutagenesis and carcinogenesis in humans. Recently, we developed a novel technique to detect multiple known or unknown DNA adducts simultaneously by using LC-MS/MS (*23, 24*). This approach, named the DNA adductome approach, monitors the neutral loss of 2′-deoxyribose from positively ionized 2′-deoxynucleoside adducts over a certain range of transitions. A variety of DNA adducts detected in DNA samples can be presented and compared by creating an adductome map showing LC retention time, mass-to-charge ratio (*m/z*), and relative peak intensity of each potential DNA adduct. In this study, we applied the DNA adductome approach to several human pulmonary DNA specimens and identified major DNA adducts on the adductome maps. Interestingly, 4-ONE- and 4-OHE-related DNA adducts were found to be major adducts in at least one pulmonary DNA sample, and they were also detected in other DNA samples. We also analyzed the levels of 4-ONE- and 4-OHE-related DNA adducts in various organs of different individuals by using LC-MS/MS. The lesions were found to be widely distributed, with some being present in significant amounts, suggesting that they could be important causative factors in human disease.

Experimental Procedures

Human Autopsy Tissues. Human autopsy tissue samples were collected at Hamamatsu University School of Medicine, Japan, and the study design was approved by the Institutional Review Board of Hamamatsu University School of Medicine (18−4). Sixty-eight samples were obtained from organs of 26 deceased persons, including the colon ($n = 6$), liver ($n = 19$), lung ($n = 12$), pancreas ($n = 9$), spleen ($n = 9$), kidney ($n = 9$), heart ($n = 2$), and small intestine ($n = 2$). The samples were taken within 24 h after death and frozen at −80 °C until DNA extraction. The ages of the subjects (17 males and 9 females) ranged from 26 to 90. Seventeen of them had malignancies as backgrounds, and final remarkable circulatory failures (shock, massive hemorrhage, and sepsis) were validated both clinically and pathologically in 6 cases. Detailed properties of the patients are listed in Supporting Information, Table S-1.

DNA Adduct Standards and Stable Isotope Standards. 4-ONE- and 4-OHE-related DNA adducts (HεdC, HεdA, HεdG, BεdC, BεmedC, BεdA, and BεdG) were synthesized according to previously published methods (*16–20*). The stereoisomers α-*S*- and α-*R*-methyl-γ-hydroxy-1,N^2-propano-2′-deoxyguanosine (CdG_1, CdG_2), 8-hydroxy-1,N^2-propanodeoxyguanosine (8-OH-AdG), and the two stereoisomers of 6-hydroxy-1,N^2-propanodeoxyguanosine (6-OH-AdG_1 and 6-OH-AdG_2) were prepared as previously described (*24*). 8-OxodG and εdA were obtained from Sigma Aldrich Japan (Japan). [U-$^{15}N_5$]-8-oxodG was kindly provided by Dr. Shinya Shibutani, State University of New York, Stony Brook, NY, [$^{15}N_5$, $^{13}C_{10}$]-2-(2′-deoxyguanosine-8-yl)-3-aminobenzanthrone ([$^{15}N_5$, $^{13}C_{10}$]-C8-C2-ABA) was kindly provided by Dr. Takeji Takamura, Kanagawa Institute of Technology, Japan, and other DNA adduct stable isotope standards were synthesized according to previously described methods using [U-$^{15}N_5$]- or [U-$^{15}N_3$]-deoxynucleosides purchased from Cambridge Isotope Laboratories (Andover, MA).

DNA Purification and Hydrolysis. Genomic DNA was isolated and purified from human autopsy samples by using a Gentra Puregene Tissue Kit (QIAGEN, Valencia, CA). DNA extraction was undertaken according to the protocol provided by the manufacturer, with the addition of desferroxamine to all solutions to a final concentration of 0.1 mM.

For DNA adductome analysis, isolated DNA was enzymatically digested as follows: each DNA sample (100 μg) was mixed with 54 μL of digestion buffer (17 mM sodium succinate and 8 mM calcium chloride, pH 6.0) containing 67.5 units of micrococcal nuclease (Worthington, Lakewood, NJ) and 0.255 units of spleen phosphodiesterase (Worthington, Lakewood, NJ). After 3 h of incubation at 37 °C, 3 units of alkaline phosphatase (Sigma-Aldrich, St. Louis, MO), 30 μL of 0.5 M Tris-HCl (pH 8.5), 15 μL of 20 mM zinc sulfate, and 101 μL of Milli-Q water were added, and the mixture were incubated for another 3 h at 37 °C. After this incubation, the mixture was concentrated to 10−20 μL by a Speed-Vac concentrator, and 100 μL of methanol was added to precipitate the protein. After centrifugation, the methanol fraction (supernatant) was transferred to a new Eppendorf tube. The precipitate was extracted with 100 μL of methanol, and the methanol fractions were combined and evaporated to dryness.

For adduct quantification analysis, the DNA sample (50 μg) was mixed with 18 μL of digestion buffer (17 mM sodium succinate and 8 mM calcium chloride, pH 6.0) containing 22.5 units of micrococcal nuclease (Worthington, Lakewood, NJ) and 0.075 units of spleen phosphodiesterase (Worthington, Lakewood, NJ) and 10 units of stable isotope-labeled DNA adduct internal standards mix, including 27.8 nM [U-$^{15}N_5$]-8-oxodG, and 1.1 nM [U-$^{15}N_5$]-εdA, [U-$^{15}N_5$]-CdG_1, [U-$^{15}N_5$]-CdG_2, [U-$^{15}N_5$]-8-OH-AdG, [U-$^{15}N_3$]-HεdC, [U-$^{15}N_5$]-HεdA, [U-$^{15}N_5$]-HεdG, [U-$^{15}N_3$]-BεdC, and [U-$^{15}N_5$]-BεdA. After 3 h of incubation at 37 °C, 3 units of alkaline phosphatase (Sigma-Aldrich, St. Louis, MO), 10 μL of 0.5 M Tris-HCl (pH 8.5), 5 μL of 20 mM zinc sulfate, and 67 μL of Milli-Q water were added, and the mixture were incubated for another 3 h at 37 °C. After this incubation, the mixture was concentrated to 10−20 μL by a Speed-Vac concentrator, and 100 μL of methanol was added to precipitate the protein. After centrifugation, the methanol fraction (supernatant) was transferred to a new Eppendorf tube. The precipitate was extracted with 100 μL of methanol, and the methanol fractions were combined and evaporated to dryness.

DNA Adductome Analysis. Digested DNA used for adductome analysis was redissolved in 120 μL of 30% dimethyl sulfoxide containing 23 nM [$^{15}N_5$, $^{13}C_{10}$]-C8-C2-ABA as the internal standard and then subjected to DNA adductome analysis similar to that described by Kanaly et al. (*24*). Briefly, adductome analysis was carried out using a Quattro Ultima Pt triple stage quadrupole mass spectrometer (Waters-Micromass, Milford, MA) equipped with a Shimadzu LC system (Shimadzu, Japan). An aliquot of digested DNA sample (10 μL) was injected and separated by a Shim-pack XR-ODS column (3.0 mm × 75 mm, Shimadzu, Japan). The column was eluted in a linear gradient of 5% to 80% methanol in water from 0 to 40 min and kept in 80% methanol in water from 40 to 45 min at a flow rate of 0.2 mL/min. Multi-reaction monitoring (MRM) was performed in positive ion mode using nitrogen as the nebulizing gas. Experimental conditions were set as follows: ion source temperature, 130 °C; desolvation temperature, 380 °C; cone voltage, 35 V; collision energy, 15 eV; desolvation gas flow rate, 700 L/h; cone gas flow rate, 35 L/h; collision gas, argon. The strategy was designed to detect the neutral loss of 2′-deoxyribose from positively ionized 2′-deoxynucleoside adducts by monitoring the samples transmitting their $[M + H]^+ \rightarrow [M + H - 116]^+$ transitions. For each DNA sample, 241 MRM transitions were monitored over the *m/z* range from transition *m/z* 250 → 134 to transition 492 → 376. For each sample injection, a total of 31 channels were monitored simultaneously with one channel for each injection reserved to monitor the internal standard [$^{15}N_5$, $^{13}C_{10}$]-C8-C2-ABA at transition *m/z* 526 → 405. Each sample was injected 8 times to complete the monitoring of 241 MRM transitions. Transitions of normal deoxynucleosides, including 252 → 136 ([dA

+ H]$^+$) and 268 → 152 ([dG + H]$^+$), were not monitored in the adductome analysis.

Relative peak intensity of each potential DNA adduct was calculated as follows: (the peak area of the potential DNA adduct)/(the peak area of the internal standard)/(the amount of 2′-deoxyguanosine (dG)). The amount of dG in each DNA sample was estimated by monitoring the dG peak area at 254 nm using the Shimazu SPD-10Avp UV−visible detector connected in series with the LC/MS/MS. The relative peak intensity was plotted as a bubble chart in which the horizontal axis was retention time and the vertical axis is *m/z*. Sodium and potassium adducts of normal deoxynucleosides or other corresponding peaks, such as those detected in the retention times of 9.3−9.5 min (dC), 10.2−10.4 min (dG), 11.2−11.4 min (dT), and 14.0−14.2 min (dA), were not included in the plot.

DNA Adduct Quantification. The digested DNA sample used for quantification was resuspended in 50 μL of 30% dimethyl sulfoxide before LC-MS/MS analysis. An aliquot (20 μL) was injected and separated by the Shim-pack XR-ODS column, eluted in a linear gradient of 5% to 30% methanol in water from 0 to 27 min, 30% to 80% from 27 to 35 min, then kept in 80% from 35 to 40 min at a flow rate of 0.2 mL/min. For the quantification of 4-ONE-derived DNA adducts, HεdC, HεdG, and HεdA, another HPLC-gradient condition was employed because of the high hydrophobicity of these compounds. A remaining aliquot (20 μL) was injected and separated by the same column, eluted in a linear gradient of 45% to 90% methanol in water from 0 to 20 min at a flow rate of 0.2 mL/min. Experimental conditions were identical to those set for adductome analysis except that the cone voltage and collision energy were different for different DNA adducts. The collision energies and characteristic reactions monitored for the different DNA adducts are as follows (cone voltage (V), collision energy (eV), base ionS → product ion): [U-$^{15}N_5$]-8-oxodG (40, 12, 288.8 → 172.8), [U-$^{15}N_5$]-εdA (35, 14, 280.9 → 164.9), [U-$^{15}N_5$]-CdG_1 and [U-$^{15}N_5$]-CdG_2 (35, 10, 343.0 → 227.0), [U-$^{15}N_5$]-8-OH-AdG (35, 10, 329.3 → 213.3), [U-$^{15}N_3$]-HεdC (35, 10, 367.0 → 251.0), [U-$^{15}N_5$]-HεdA (35, 10, 393.0 → 277.0), [U-$^{15}N_5$]-HεdG (35, 10, 409.0 → 293.0), [U-$^{15}N_3$]-BεdC (35, 10, 324.8 → 208.6), and [U-$^{15}N_5$]-BεdA (35, 10, 351.0 → 234.8), 8-oxodG (40, 12, 283.8 → 167.8), εdA (35, 14, 275.9 → 159.9), CdG_1 and CdG_2 (35, 10, 338.0 → 222.0), 8-OH-AdG, 6-OH-AdG_1, and 6-OH-AdG_2 (35, 10, 324.3 → 208.3), HεdC (35, 10, 364.0 → 248.0), HεdA (35, 10, 388.0 → 272.0), HεdG (35, 10, 404.0 → 288.0), BεdC (35, 10, 321.8 → 205.6), BεmedC (35, 20, 335.9 → 220.0), and BεdA (35, 10, 351.0 → 234.8) and BεdG (35, 20, 362.0 → 245.9).

The amount of each DNA adduct was quantified by calculating the peak area ratio of the target DNA adduct and its specific internal standard ([U-$^{15}N_3$]-BεdC was used for BεdC and BεmedC, and [U-$^{15}N_5$]-BεdA was used for BεdA and BεdG). Calibration curves were obtained by using authentic standards spiked with isotope internal standards. The concentration of dG in each DNA sample was also monitored as described in the DNA Adductome Analysis section. The number of DNA adducts per 10^8 bases was calculated by the following equation: number of DNA adducts per 10^8 bases = adduct level (fmol/μmol dG) × 0.218(μmol dG/μmol dN) × 10^{-1}, as described previously (*25*).

Results

Adductome Analysis of DNA Extracted from Human Lung Autopsy Tissues. We applied adductome analysis to DNA extracted from four human lung autopsy samples to simultaneously detect a variety of known and unknown DNA adducts in human pulmonary DNA. Although adductome analysis is semiquantitative, this analysis would help to grasp a complete picture of the DNA adducts in human samples. Several peaks were identified as corresponding to known DNA adducts by showing identical *m/z* and LC retention times to DNA adduct standards. Figure 1 shows the adductome maps of two human pulmonary DNA samples having different patterns of DNA

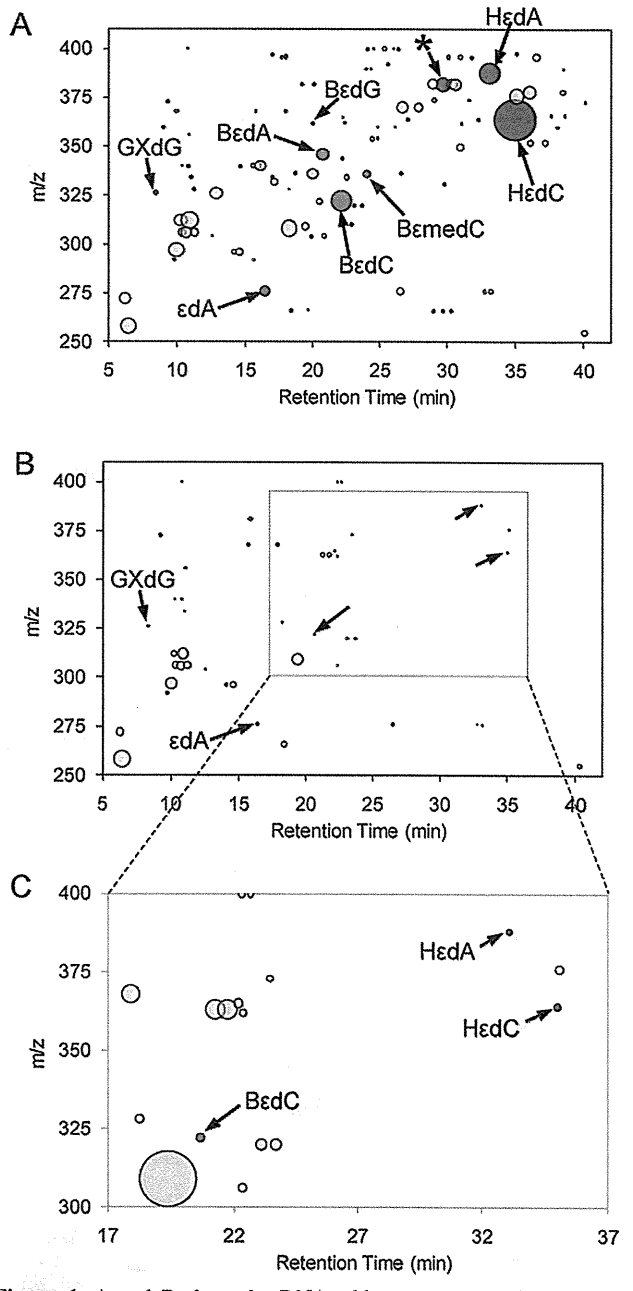

Figure 1. A and B show the DNA adductome maps of two human pulmonary DNA samples from different individuals, and C is a close-up of a selected area in B. Each circle represents one DNA adduct candidate detected by adductome analysis using LC-MS/MS. HPLC retention time, mass to charge ratio (*m/z*), and relative intensity (shown by the size of each circle, which is proportional to the peak area of each DNA adduct candidate divided by the peak area of the internal standard and the amount of 2′-deoxyguanosine) of each DNA adduct candidate can be found on the maps. Blue circles represent corresponding peaks of 4-ONE-related DNA adducts, while orange circles represent 4-OHE-related DNA adducts. Green circles are the other lipid-peroxidation derived DNA adducts, and yellow circles represent unidentified peaks. GXdG: 1,N^2-glyoxyal-dG. *: heptanone-ethano-2′-deoxycytidine.

adduct composition. Numerous DNA adducts can be seen in Figure 1A, and LPO-induced DNA adducts were detected as major peaks, including HεdC, HεdA, BεdC, BεdA, BεmedC, BεdG, εdA, and 1,N^2-glyoxal-dG. Although fewer DNA adducts were found in the sample represented in Figure 1B, LPO-induced DNA adducts derived from 4-ONE and 4-OHE (i.e., HεdC, HεdA, and BεdC) were nonetheless detected. Adductome maps of two other human pulmonary DNA samples have patterns similar to that shown in Figure 1B (data not shown),

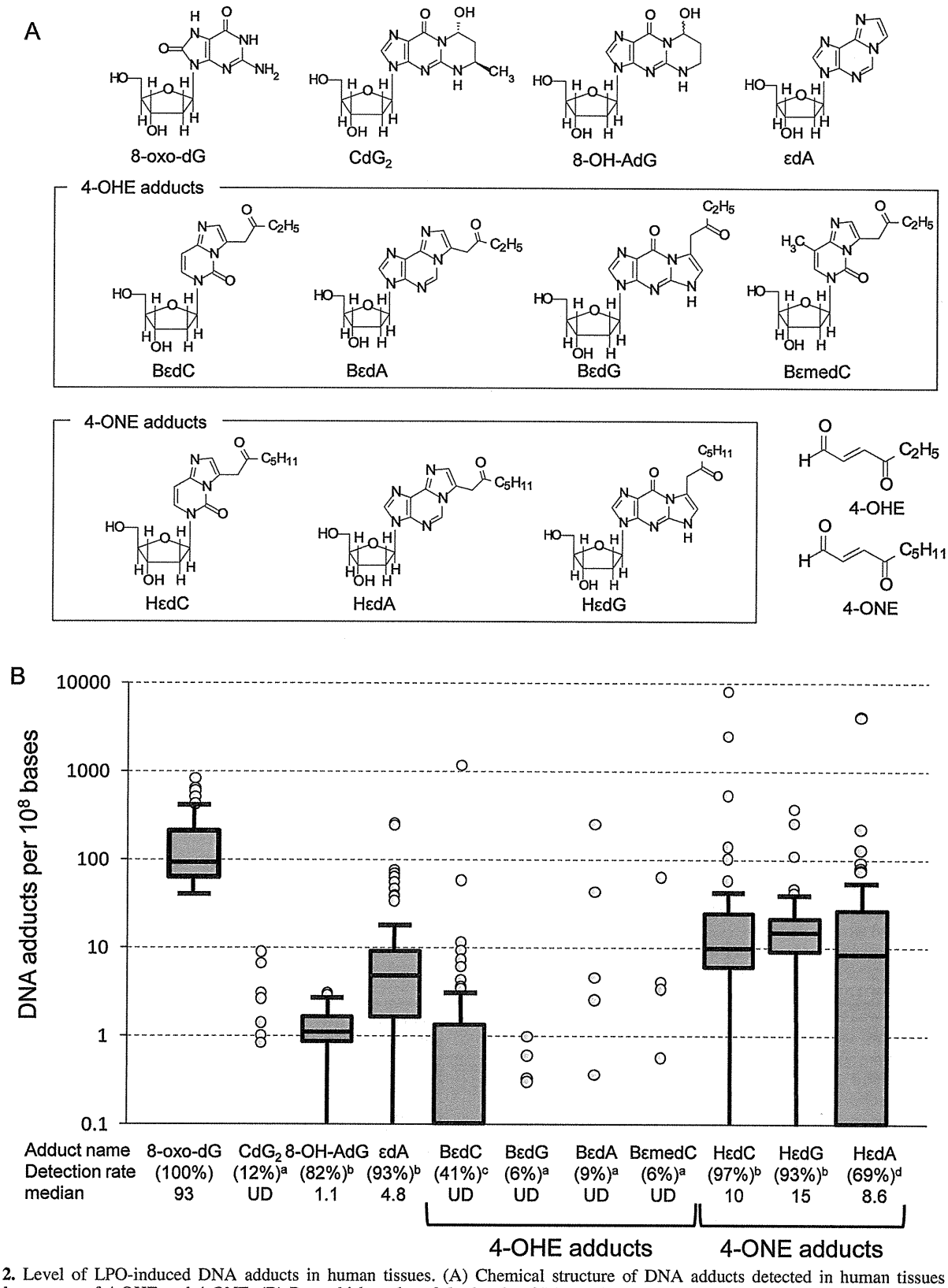

Figure 2. Level of LPO-induced DNA adducts in human tissues. (A) Chemical structure of DNA adducts detected in human tissues and the chemical structure of 4-OHE and 4-ONE. (B) Box-whisker plot of the levels of DNA adducts detected in human autopsy tissues, including the colon, liver, lung, pancreas, spleen, kidney, heart, and small intestine (n = 68). The boxes indicate the 75th percentile, the median, and the 25th percentile. The ends of the whiskers indicate the minimum and maximum data values unless outliers are present, in which case the whiskers extend to a maximum of 1.5 times the interquartile range. Circles above the whisker indicate outliers. Although crotonaldehyde-induced CdG_1 and acrolein-induced 6-OH-AdG_1 and 6-OH-AdG_2 were also monitored, we could not detect those adducts. Detected rate and median are shown under each DNA adduct. UD: under the detection limit. a, 75th percentile was UD; b, minimum was UD; c, median was UD; d, 25th percentile was UD.

indicating that DNA adducts induced by 4-ONE and 4-OHE are often formed in human lungs.

Detection of 4-ONE- and 4-OHE-Induced DNA Adducts in Human Autopsy Tissues. To elucidate whether the levels of

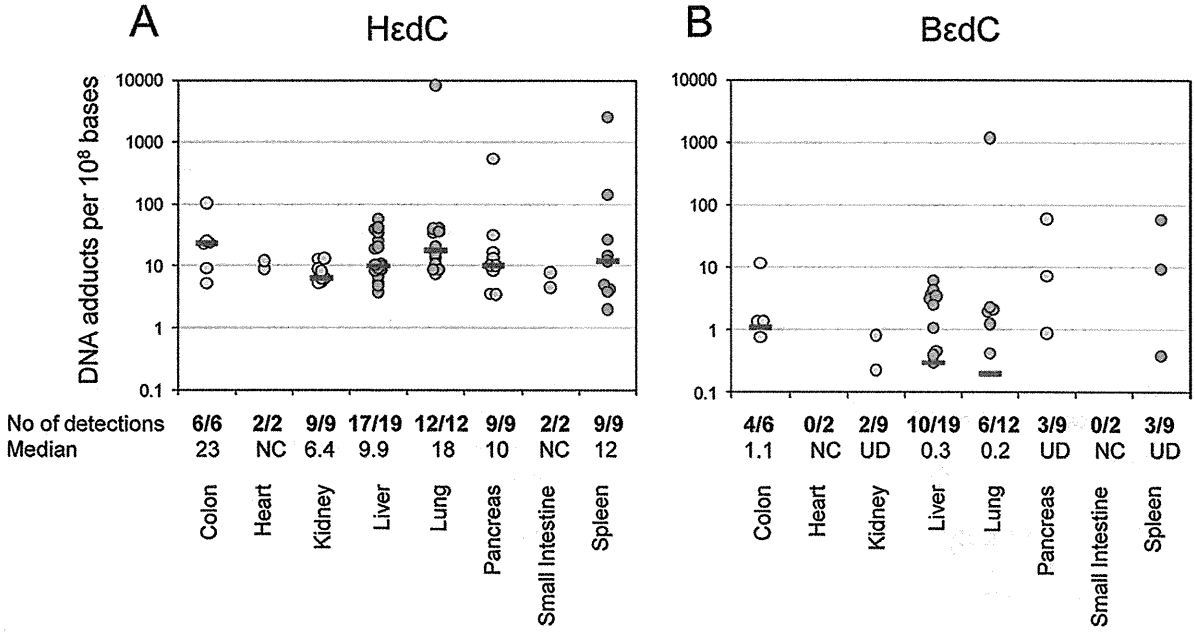

Figure 3. DNA adduct levels of HεdC and BεdC detected in various human autopsy tissues. Data from the DNA of 6 colons, 2 hearts, 9 kidneys, 19 livers, 12 lungs, 9 pancreases, 2 small intestines, and 9 spleens were plotted as circles, and the blue bars indicate the median values. NC: not calculated because the sample number was only 2. UD: median was under the detection limit.

4-ONE- and 4-OHE-related DNA adducts are comparable to those of other DNA adducts frequently found in human tissues, we measured the levels of various DNA adducts by using LC-MS/MS in 68 human autopsy specimens obtained from 26 persons, including samples of colon (n = 6), liver (n = 19), lung (n = 12), pancreas (n = 9), spleen (n = 9), kidney (n = 9), heart (n = 2), and small intestine (n = 2). The approximate detection limit of the DNA adducts (in the case that 50 μg of DNA was digested and 40% of the portion was injected to the LC/MS/MS) were as follows: 8-oxodG (1.65 adduct per 10^8 bases), εdA (0.17), CdG_1 and CdG_2 (0.17), 8-OH-AdG (0.05), 6-OH-AdG_1 and 6-OH-AdG_2 (0.08), HεdC (0.33), HεdA (1.65), HεdG (1.65), BεdC (0.17), BεmedC (0.17), and BεdA (0.83) and BεdG (0.83) (Supporting Information Figures S-2 and S-3, Table S-8), and the calibration curves of each DNA adducts are shown in Supporting Information, Figure S-4. We could detect the target DNA adducts in several human tissue samples (the representative chromatographs are shown in Supporting Information, Figures S-5, S-6, and S-7). The results revealed that the levels of target DNA adducts varied considerably among individuals or organs (Figure 2 and Supporting Information, Table S-8). Figure 2 shows the DNA adduct levels of the oxidative lesion 8-oxodG as well as the LPO-related lesions CdG_2, 8-OH-AdG, εdA, BεdC, BεdG, BεdA, BεmedC, HεdC, HεdG, and HεdA. 8-OxodG was detected in all autopsy tissues, and high detection rates were also found for εdA (93%) and 8-OH-AdG (82%). 4-ONE-related DNA adducts were also frequently detected in various tissue samples: total detection rates for HεdC, HεdG, and HεdA were 97%, 93%, and 63%, respectively. 4-OHE-related BεdC, having a total detection rate of 41%, was commonly found in the colon, liver, and lung, with detection rates higher than 50%. However, the other 4-OHE-related adducts, BεdG, BεdA, and BεmedC, showed lower detection rates of 6%, 9%, and 6%, respectively. The detection rate of the crotonaldehyde-derived DNA adduct CdG_2 was 12%. Although crotonaldehyde-induced CdG_1 and acrolein-induced 6-OH-AdG_1 and 6-OH-AdG_2 were also monitored, we could not detect those adducts in any sample. The level of each DNA adduct per 10^8 bases ranged as follows: 8-oxo-dG, 41.6−837 (median 93.2); CdG_2, not detected (ND) to 8.98 (median was under the detection limit); 8-OH-AdG, ND to 3.04 (median 1.14); εdA, ND to 259 (median 4.83); BεdC, ND to 1186 (median was under the detection limit); BεdG, ND to 0.99 (median was under the detection limit; BεdA, ND to 254 (median was under the detection limit); BεmedC, ND to 63.8 (median was under the detection limit); HεdC, ND-8204 (median 10.3); HεdG, ND to 377 (median 15.0); and HεdA, ND to 4186 (median 8.63).

Adduct Levels of HεdC and BεdC in Different Organs. As shown in Figure 3, DNA adduct levels of HεdC and BεdC range broadly in different organs. HεdC was detected in all tissue samples except for two liver specimens, whereas BεdC was detected in the colon, kidney, liver, lung, spleen, and pancreas. The median level of HεdC in different organs ranged from 6.4 (kidney) to 23 (colon) adducts per 10^8 bases, whereas the median of BεdC was 1 or 2 orders of magnitude lower. However, an extremely high level of HεdC (more than 100 adducts per 10^8 bases) was found in one colon, one lung, one pancreas and two spleen DNA samples, all from different individuals. Also, an extremely high level of BεdC was observed in one lung DNA sample, the same one that showed a high HεdC level as described above. The results suggest that 4-ONE- and 4-OHE-related DNA adducts are widely distributed in various tissues.

Figure 4 shows the correlations of BεdC, εdA, and 8-oxodG with HεdC in human tissue autopsy samples. The DNA adduct level of HεdC was strongly correlated to LPO-induced BεdC (R^2 = 0.94) and εdA (R^2 = 0.70), but no correlation could be seen between HεdC and the oxidative damage-related lesion 8-oxodG (R^2 = 0.02).

Discussion

In this study, we clearly demonstrated that DNA adducts derived from 4-ONE and 4-OHE occur commonly in human tissues. The levels of the 4-ONE-related DNA adducts HεdC, HεdA, and HεdG in human tissue samples were similar to each other (Supporting Information, Figure S-9), and their median values were 2- to 3-fold higher than that of εdA. However, the 4-OHE-related adducts BεdC, BεmedC, BεdA, and BεdG were detected at lower levels and frequencies; in most samples, their

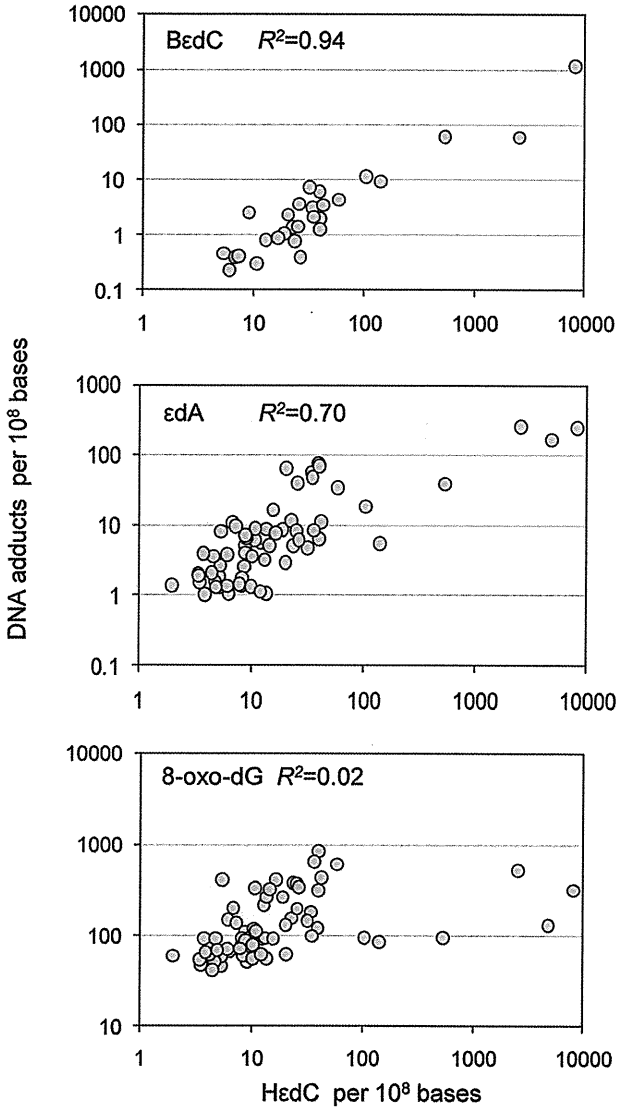

Figure 4. Correlations among DNA adduct levels of HεdC vs BεdC, εdA, and 8-oxodG. R^2: coefficient of determination. For the R^2 calculation, not detected data was treated as 0.

levels were similar to that of crotonaldehyde-derived CdG_2 or acrolein-derived 8-OH-AdG. Importantly, in some cases, the levels of these 4-ONE- and 4-OHE-derived DNA adducts were comparable to or even higher than that of the most abundant DNA adduct, 8-oxo-dG. Thus, these recently recognized DNA adducts may be an important source of somatic mutations and could significantly contribute to cancer formation in humans.

The tissues adjacent to those taken for adductome analysis were microscopically examined for the absence of tumor cells. The histological findings varied in terms of inflammation, not otherwise specified. Details of histological characteristics and their relationship to the DNA adducts level are under investigation.

Mutagenic properties of HεdC have been demonstrated in mammalian cell lines and *Escherichia coli* (*26, 27*). Pollack et al. (*26*) reported that in human cell lines HεdC blocked DNA synthesis and also miscoded markedly during the replication of a shuttle vector site-specifically modified with HεdC. The miscoding frequency was higher than 90%, and dT and dA were preferentially inserted opposite the lesion in human cells. HεdC was also shown to be genotoxic in a similar host-vector system consisting of mouse fibroblasts and a replicating plasmid bearing a site-specific HεdC (*25*). Moreover, the results indicated that the Y family DNA polymerases η, κ, and ι preferentially catalyzed the insertion of dT opposite HεdC, whereas an unidentified DNA polymerase was suggested to catalyze the insertion of dA opposite HεdC (*27*). Information about the potential mutagenic properties of the other 4-ONE- and 4-OHE-derived DNA adducts found in human autopsy tissues is still unavailable; thus, further studies concerning the mutagenicity and DNA repair pathways of these newly identified DNA adducts are necessary.

Human tissues could be exposed to 4-ONE and 4-OHE endogenously and exogenously. The endogenous formation of 4-ONE and 4-OHE is via the oxidation of ω6- and ω3-PUFAs in tissues. Because all bodily tissues contain both ω6- and ω3-PUFAs, 4-ONE and 4-OHE could be produced simultaneously under oxidative stress conditions. The near-perfect correlation between the levels of HεdC and BεdC (R^2 = 0.94) shown in Figure 4 strongly suggests that there is endogenous and simultaneous formation of 4-ONE- and 4-OHE-derived DNA adducts. According to the slope of the regression curve, the level of HεdC was about 7 times greater than that of BεdC. This also supports the endogenous-formation hypothesis because in all tissues except the brain, the total concentration of ω6- PUFAs is several times higher than that of ω3-PUFAs (*28, 29*).

However, no correlation was observed between the level of HεdC and the level of the oxidative DNA lesion 8-oxo-dG (Figure 4). This discrepancy may be explained by the contribution of enzymatic formation pathways to 4-ONE. For example, Blair's group demonstrated that overexpression of cyclooxygenase-2 (COX-2) increased the level of 4-ONE-derived DNA adducts in both rat intestinal epithelial cells (*30*) and the small intestine of C57BL/6J APC^{min} mice (*31*). COX-2 is an enzyme that is responsible for the formation of the important biological mediator prostaglandin H2. COX-2 can also convert arachidonic acid into 15(*S*)-hydroperoxy-5*Z*,8*Z*,11*Z*,13*E*-eicosatetraenoic acid (15-HPETE), which undergoes homolytic decomposition to the DNA-reactive bifunctional electrophiles 4-hydroperoxy-2(*E*)-nonenal (HPNE), 4,5-epoxy-2(*E*)-decenal (EDE), 4-HNE, and 4-ONE (*31*). 4-ONE is also produced enzymatically from arachidonic acid by the 5-lipoxygenase (5-LO)-related pathway (*32*). 5-LO is an enzyme that is responsible for the formation of leukotriene A_4. The precursor of leukotriene A_4, 5(*S*)-hydroperoxy-6*E*,8*Z*,11*Z*,14*Z*-eicosatetraenoic acid (5(*S*)-HPETE), generated from arachidonic acid by 5-LO, decomposes to form 4-ONE and HPNE (*32*). The considerably good correlation between the DNA adduct levels of HεdC and εdA, as described in Figure 4 (R^2 = 0.70), also suggests the involvement of this metabolic pathway, because εdA is known to be produced by HPNE and EDE (*31*). If 4-OHE is also produced enzymatically from abundant ω3-PUFAs such as docosahexaenoic acid, this would help to explain why the level of BεdC nearly perfectly correlates with the level of HεdC but the level of 8-oxo-dG does not. Further study is needed to elucidate this point.

The exogenous sources of 4-ONE and 4-OHE are foods and cooking vapor. Kasai and Kawai reported that several types of cooked fishes and cooking oils contain 4-OHE in the range of a few to tens of micrograms per gram (*21*). They further reported that the cooking vapor emitted during fish broiling also contains 4-OHE (*21*). In an animal experiment, orally administered 4-OHE resulted in the formation of BεdC, BεdG, and BεmedC in cells of the gastrointestinal tract, but no increase in the level of DNA adducts was observed in the liver and kidney (*19*), indicating that, except for the gastrointestinal tract, the oral route is probably not a significant source of 4-OHE. However, the

impact of cooking vapor in terms of the formation of DNA adducts in pulmonary tissues remains to be resolved.

In conclusion, DNA adducts caused by 4-ONE and 4-OHE are ubiquitous in various human tissues, and even predominant in some cases. It is very likely that these DNA adducts cause somatic mutations and cancers, contribute to aging, and have other adverse effects related to DNA damage. Further studies of their exposure routes and biological properties should be carried out to elucidate the impact of these DNA lesions on human health.

Acknowledgment. We thank H. Igarashi and T. Kamo of Hamamatsu University School of Medicine for assistance in collecting the samples. This work was supported by KAKENHI (20014007, 18181883 and 18014009); Grants-in-aid for cancer research from MHLW, Japan; the National Science Council, Taiwan (NSC 98-2221-E-006-020-MY3); NEDO, Japan; and the Smoking Research Foundation.

Supporting Information Available: Properties of the patients; sensitivity of LC/MS/MS analysis for each DNA adduct (1 and 2); calibration curves of each DNA adduct; representative chromatographs of DNA adducts, 4-OHE-derived DNA adducts, and 4-ONE-derived DNA adducts in human spleen DNA; DNA adducts level in human tissues; and correlations among the 4-ONE-derived DNA adduct level of HεdC vs HεdA (A) and HεdG (B). This material is available free of charge via the Internet at http://pubs.acs.org.

References

(1) Cajelli, E., Ferraris, A., and Brambilla, G. (1987) Mutagenicity of 4-hydroxynonenal in V79 Chinese hamster cells. *Mutat. Res. 190*, 169–171.

(2) Nath, R. G., Ocando, J. E., and Chung, F. L. (1996) Detection of 1, N2-propanodeoxyguanosine adducts as potential endogenous DNA lesions in rodent and human tissues. *Cancer Res. 56*, 452–456.

(3) Guillen, M. D., and Goicoechea, E. (2008) Toxic oxygenated alpha-,beta-unsaturated aldehydes and their study in foods: a review. *Crit. Rev. Food Sci. Nutr. 48*, 119–136.

(4) Blair, I. A. (2008) DNA adducts with lipid peroxidation products. *J. Biol. Chem. 283*, 15545–15549.

(5) Markesbery, W. R., and Carney, J. M. (1999) Oxidative alterations in Alzheimer's disease. *Brain Pathol. 9*, 133–146.

(6) Williams, M. V., Wishnok, J. S., and Tannenbaum, S. R. (2007) Covalent adducts arising from the decomposition products of lipid hydroperoxides in the presence of cytochrome c. *Chem. Res. Toxicol. 20*, 767–775.

(7) De Bont, R., and van Larebeke, N. (2004) Endogenous DNA damage in humans: a review of quantitative data. *Mutagenesis 19*, 169–185.

(8) Nair, J., De Flora, S., Izzotti, A., and Bartsch, H. (2007) Lipid peroxidation-derived etheno-DNA adducts in human atherosclerotic lesions. *Mutat. Res. 621*, 95–105.

(9) Wang, H. T., Zhang, S., Hu, Y., and Tang, M. S. (2009) Mutagenicity and Sequence Specificity of Acrolein-DNA Adducts. *Chem. Res. Toxicol. 22*, 511–517.

(10) Uchida, K. (2003) 4-Hydroxy-2-nonenal: a product and mediator of oxidative stress. *Prog. Lipid Res. 42*, 318–343.

(11) Schaur, R. J. (2003) Basic aspects of the biochemical reactivity of 4-hydroxynonenal. *Mol. Aspects Med. 24*, 149–159.

(12) Feng, Z., Hu, W., and Tang, M. S. (2004) Trans-4-hydroxy-2-nonenal inhibits nucleotide excision repair in human cells: a possible mechanism for lipid peroxidation-induced carcinogenesis. *Proc. Natl. Acad. Sci. U.S.A. 101*, 8598–8602.

(13) McGrath, L. T., McGleenon, B. M., Brennan, S., McColl, D., Mc, I. S., and Passmore, A. P. (2001) Increased oxidative stress in Alzheimer's disease as assessed with 4-hydroxynonenal but not malondialdehyde. *Q. J. Med. 94*, 485–490.

(14) Feng, Z., Hu, W., Amin, S., and Tang, M. S. (2003) Mutational spectrum and genotoxicity of the major lipid peroxidation product, trans-4-hydroxy-2-nonenal, induced DNA adducts in nucleotide excision repair-proficient and -deficient human cells. *Biochemistry 42*, 7848–7854.

(15) Zarkovic, N. (2003) 4-hydroxynonenal as a bioactive marker of pathophysiological processes. *Mol. Aspects Med. 24*, 281–291.

(16) Rindgen, D., Nakajima, M., Wehrli, S., Xu, K., and Blair, I. A. (1999) Covalent modifications to 2′-deoxyguanosine by 4-oxo-2-nonenal, a novel product of lipid peroxidation. *Chem. Res. Toxicol. 12*, 1195–1204.

(17) Rindgen, D., Lee, S. H., Nakajima, M., and Blair, I. A. (2000) Formation of a substituted 1, N(6)-etheno-2′-deoxyadenosine adduct by lipid hydroperoxide-mediated generation of 4-oxo-2-nonenal. *Chem. Res. Toxicol. 13*, 846–852.

(18) Pollack, M., Oe, T., Lee, S. H., Silva Elipe, M. V., Arison, B. H., and Blair, I. A. (2003) Characterization of 2′-deoxycytidine adducts derived from 4-oxo-2-nonenal, a novel lipid peroxidation product. *Chem. Res. Toxicol. 16*, 893–900.

(19) Kasai, H., Maekawa, M., Kawai, K., Hachisuka, K., Takahashi, Y., Nakamura, H., Sawa, R., Matsui, S., and Matsuda, T. (2005) 4-oxo-2-hexenal, a mutagen formed by omega-3 fat peroxidation, causes DNA adduct formation in mouse organs. *Ind. Health 43*, 699–701.

(20) Maekawa, M., Kawai, K., Takahashi, Y., Nakamura, H., Watanabe, T., Sawa, R., Hachisuka, K., and Kasai, H. (2006) Identification of 4-oxo-2-hexenal and other direct mutagens formed in model lipid peroxidation reactions as dGuo adducts. *Chem. Res. Toxicol. 19*, 130–138.

(21) Kasai, H., and Kawai, K. (2008) 4-oxo-2-hexenal, a mutagen formed by omega-3 fat peroxidation: occurrence, detection and adduct formation. *Mutat. Res. 659*, 56–59.

(22) Kawai, K., Chou, P. H., Matsuda, T., Inoue, M., Aaltonen, K., Savela, K., Takahashi, Y., Nakamura, H., Kimura, T., Watanabe, T., Sawa, R., Dobashi, K., Li, T. S., and Kasai, H. (2010) DNA modifications by the ω-3 lipid peroxidation-derived mutagen 4-oxo-2-hexenal in vitro and their analysis in mouse and human DNA. *Chem. Res. Toxicol. 23*, 630–636.

(23) Kanaly, R. A., Hanaoka, T., Sugimura, H., Toda, H., Matsui, S., and Matsuda, T. (2006) Development of the adductome approach to detect DNA damage in humans. *Antioxid. Redox Signaling 8*, 993–1001.

(24) Kanaly, R. A., Matsui, S., Hanaoka, T., and Matsuda, T. (2007) Application of the adductome approach to assess intertissue DNA damage variations in human lung and esophagus. *Mutat. Res. 625*, 83–93.

(25) Matsuda, T., Yabushita, H., Kanaly, R. A., Shibutani, S., and Yokoyama, A. (2006) Increased DNA damage in ALDH2-deficient alcoholics. *Chem. Res. Toxicol. 19*, 1374–1378.

(26) Pollack, M., Yang, I. Y., Kim, H. Y., Blair, I. A., and Moriya, M. (2006) Translesion DNA Synthesis across the heptanone−etheno-2′-deoxycytidine adduct in cells. *Chem. Res. Toxicol. 19*, 1074–1079.

(27) Yang, I. Y., Hashimoto, K., de Wind, N., Blair, I. A., and Moriya, M. (2009) Two distinct translesion synthesis pathways across a lipid peroxidation-derived DNA adduct in mammalian cells. *J. Biol. Chem. 284*, 191–198.

(28) Tahin, Q. S., Blum, M., and Carafoli, E. (1981) The fatty acid composition of subcellular membranes of rat liver, heart, and brain: diet-induced modifications. *Eur. J. Biochem. 121*, 5–13.

(29) Engler, M. M., Engler, M. B., Kroetz, D. L., Boswell, K. D. B., Neeley, E., and Krassner, S. M. (1999) The effects of a diet rich in docosahexaenoic acid on organ and vascular fatty acid composition in spontaneously hypertensive rats. *Prostaglandins, Leukotrienes Essent. Fatty Acids 61*, 289–295.

(30) Lee, S. H., Williams, M. V., Dubois, R. N., and Blair, I. A. (2005) Cyclooxygenase-2-mediated DNA damage. *J. Biol. Chem. 280*, 28337–28346.

(31) Williams, M. V., Lee, S. H., Pollack, M., and Blair, I. A. (2006) Endogenous lipid hydroperoxide-mediated DNA-adduct formation in min mice. *J. Biol. Chem. 281*, 10127–10133.

(32) Jian, W., Lee, S. H., Williams, M. V., and Blair, I. A. (2009) 5-Lipoxygenase-mediated endogenous DNA damage. *J. Biol. Chem. 284*, 16799–16807.

TX100047D

Genes and Environment, Vol. 32, No. 2 pp. 21–24 (2010)

Commentary

Anticipated Mutation Assay Using Single-molecule Real-time (SMRT™) Sequencing Technology

Tomonari Matsuda[1]

Research Center for Environmental Quality Management, Kyoto University, Kyoto, Japan

(Received April 1, 2010; Revised April 19, 2010; Accepted April 20, 2010)

I describe here an anticipated mutation assay which estimates the frequency and spectrum of somatic point mutations in any genes of any samples by using SMRT™ (Single Molecule Real Time) DNA sequencing technology, which will be released in 2010. The basic concept of the mutation assay is very simple: just prepare the target template and sequence it accurately. In this paper, I propose ideas on how to make the template and how to eliminate artifactual mutations caused by damage to the DNA template.

Key words: DNA sequencer, single molecule real time (SMRT™), mutation assay, DNA adducts

Introduction

To evaluate the cancer risk of chemicals, many mutation assays have been developed, most using sophisticated genetic technologies. However, ideally, researchers want to estimate mutation frequencies in the most relevant genes such as *p53* or *APC* rather than the currently used mutational target genes such as *hprt*, *tk*, *lacZ* etc. Researchers want to analyze mutation spectra in clinically relevant samples such as human blood or tissues rather than in genetically engineered special cell lines or transgenic animals that offer convenience. The ultimate genotoxicity test would measure mutation frequencies and spectra in any gene of any sample directly. Is this possible?

Recently, second-generation DNA sequencers using DNA sequencing-by-synthesis technology have been developed, leading to dramatic increases in speed of analysis. For example, we can now access a service which can read up to 10^9 bases per day by using Roche's GS FLX DNA sequencer. Assuming that the spontaneous mutation frequency is around 10^{-8} (although nobody knows the real level), such a platform would, in principle, permit detection of point mutations at the spontaneous level. The idea of using DNA sequencers for mutation assays is now becoming a real possibility. However, it still remains difficult to realize this idea, especially in terms of accuracy and read length per single read (on average 350–450 bases).

In the mean time, development of a third-generation DNA sequencer has steadily advanced. On February 23, 2010, Pacific Biosciences, a private company developing a Single Molecule Real Time (SMRT™) DNA sequencer, finally announced that they will release the first shipments of their SMRT™ DNA sequencer to 10 institutions in the United States in the first half of 2010 (1). The company claims that the SMRT™ DNA sequencer is able to read 100 Gigabases per hour, which is at least 100 times faster than the fastest second-generation DNA sequencers. I think that this third-generation DNA sequencer will enable us to detect somatic mutations in any gene of any sample.

Overview of SMRT™ Technology

The principle of this amazing SMRT™ DNA sequencer is described on PACIFIC BIOSCIENCES's home page (www.pacficbiosciences.com) with an animated video (please see the movie before reading the following part) and in review papers (2–4). DNA sequencing is performed on SMRT™ chips, each containing thousands of 'zero-mode waveguides' (ZMWs), which are holes tens of nanometers in diameter, 20 zeptoliters in volume. In this ZMW, a single DNA polymerase molecule is immobilized at the bottom. A template single-strand DNA molecule is introduced into the ZMW and the DNA synthesis reaction is initiated with fluorescence-labeled deoxynucleotides. The deoxynucleotides (dATP, dGTP, dCTP, dTTP), each type labeled with a different colored fluorophore in their triphosphate chains, is held by the DNA polymerase molecule for tens of milliseconds, producing a bright flash of light when it is incorporated into the elongating DNA strand. The sequencer detects the light in real time at a speed of tens of incorporations per second. Since the fluorophore is attached to the terminal phosphate of the triphosphate chain of each deoxynucleotide rather than

[1]Correspondence to: Tomonari Matsuda, Research Center for Environmental Quality Management, Kyoto University, 1-2 Yumihama, Otsu, Shiga 520-0811, Japan. Tel: +81-77-527-6224, FAX: 077-524-9869, E-mail: matsuda@z05.mbox.media.kyoto-u.ac.jp

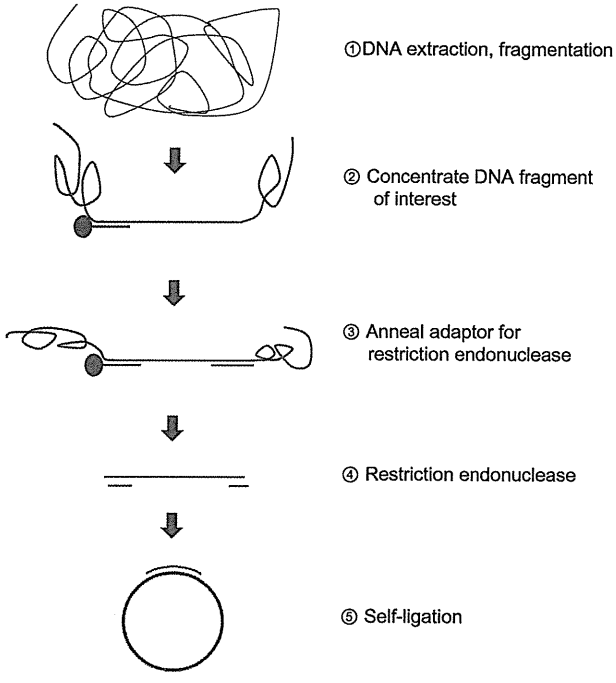

Fig. 1. Template preparation strategy of the mutation assay.

to the base, the DNA polymerase consecutively incorporates unmodified nucleotides, producing a long, natural DNA. This makes it possible to read thousands of bases in a single processive step.

Strategy for Applying SMRT™ Technology as a Mutation Assay

SMRT™'s 'single molecule real time' platform and the tremendous sequencing speed of 100 Gigabases per hour, together with the capability of long reads, should enable us to detect point mutations in any gene of any sample. The basic concept of the mutation assay is very simple: just prepare target template and sequence it accurately. To ensure accuracy of sequencing, 'circular single-stranded DNA template' is provided to conduct DNA sequencing repeatedly on the same template.

Template preparation: A target gene can be selected as one chooses. The length of the target will be around 1000 bases. As shown in Fig. 1, DNA extracted from tissues or cells of interest is digested by a restriction endonuclease. The DNA fragment containing the target sequence is concentrated by a solid-phase reagent (e.g., Dynabeads etc.), attaching the target's complementary single-strand DNA. Then an adaptor for the restriction endonuclease is annealed, followed by digestion by the restriction endonuclease. The released DNA fragment is self-ligated to form a circular single-stranded DNA with primer. The necessary amount of the starting DNA sample will depend on recovery rate of the target sequence through template preparation. Ten

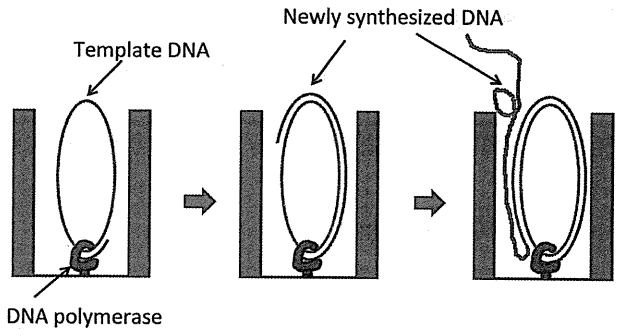

Fig. 2. Repeated sequencing by the SMRT™ DNA sequencer. The long-read property of SMRT™ enables repeated sequencing. Sequence in the circular DNA template can be read several times to ensure accuracy.

microgram of DNA will be fine if the recovery is almost 100%, because 10 microgram of DNA prepared from human cells contains 6×10^6 copies of the target sequence. Assuming that the length of the target is 1000 bases, denominator for mutation frequency will be 6×10^9 bases which will be enough to discuss spontaneous mutation frequency.

Repeated-sequencing and mutation identification: SMRT™ sequencing will enable repeated-sequencing applications. If a circular template is applied to the SMRT™ chip, the template will be read repeatedly. This will increase the accuracy of the sequence data (Fig. 2). The circular single-strand DNA template prepared as above is sequenced three or more times and a putative mutation is considered genuine only if the same mutation appears at the same position during the repeated analysis.

Effects of Abundant DNA Adducts on the Mutation Detection Strategy

Although it is an attractive strategy to detect point mutations directly using the SMRT™ DNA sequencer, it is difficult to distinguish a 'real mutation' from an artifact generated during the sequencing process. Simple polymerase errors will occur at a frequency of at least 1 error per 10^5 bases even though a high-fidelity DNA polymerase is used (3). However, this kind of error can be excluded by the repeated-sequencing strategy as described above. Assuming that the spontaneous mutation frequency is around 10^{-8}, and the fidelity of the DNA polymerase is approximately 10^{-4}, repeating the sequencing three times might be enough to eliminate this kind of artifact.

However, in the template DNA there are likely to be many DNA adducts of sample origin or produced during DNA isolation and template preparation, which could dramatically increase misincorporation rates at the damaged position. Table 1 lists abundant DNA adducts which may affect polymerase fidelity. For exam-

Table 1. Abundant DNA adducts which may cause sequencing artifacts

Adducts	Precursor	Adduct level/ 10^6 bases	Bases incorporated opposite the lesion	References
8-oxo-dG	G	1	C, A	(5)
AP site	Any bases	4	A	(6, 7)
dU	C	50	A	(8)
dI	A	1	C	(8, 9)
dX	G	0.5	C, T	(8, 10)

ple, in an *in vitro* trans-lesion DNA synthesis experiment, both dA and dC were incorporated opposite to 8-oxo-dG in a synthetic oligonucleotide template. The incorporation profile varies depending on the kind of polymerase used (5). Although information about which DNA polymerase is employed on the SMRT™ chip has not been disclosed, let us assume that the polymerase will incorporate dA opposite 8-oxo-dG in the template strand with a probability of 30%; therefore, the probability that we will misread dG as dT at the 8-oxo-dG site will be 2.7% ($=0.3\times0.3\times0.3$) after triplicate sequencing of the template. If the level of 8-oxo-dG in DNA is 1 adduct per 10^6 bases, then 2.7 artifactual mutations per 10^8 bases will occur caused by 8-oxo-dG. A similar situation is expected in the case of other abundant DNA adducts such as the apurinic/apyrimidinic (AP) site, deoxyinosine (dI) and deoxyxanthosine (dX).

Taking an optimistic view, SMRT™'s real-time detection should allow us to minimize this difficulty. DNA synthesis will be slowed down when the DNA polymerase encounters a DNA adduct. This should permit us to distinguish between a normal base site and a DNA-adducted site by monitoring the speed of DNA synthesis (Fig. 3). However, this limitation may still exist in the case of deoxyuridine (dU), which is produced by deamination of dC or incorporated into DNA opposite dA during DNA replication. Because the base-pairing properties of dU resemble those of dT, it might not be possible to distinguish dU from normal bases by the DNA synthetic speed. If this is the case, we would have to pretreat the template DNA with uracil DNA glycosidase to convert dU to an AP site before subjecting it to SMRT™ DNA sequencing.

Conclusion

As described above, applying the SMRT™ DNA sequencer to a mutation assay is very promising. Of course, there may be various technical difficulties lying in the way of development. However, in principle, this technology can shed light on somatic mutations in any genes of interest for the first time in history, which will significantly enhance our understanding of mutagenesis, tumorigenesis and aging. Also, this strategy should be very useful for risk evaluation of chemicals, because we might be able to detect mutations in oncogenes and tumor suppressor genes directly. I am looking forward to my chance to access the SMRT™ DNA sequencer to develop this mutation assay in the near future.

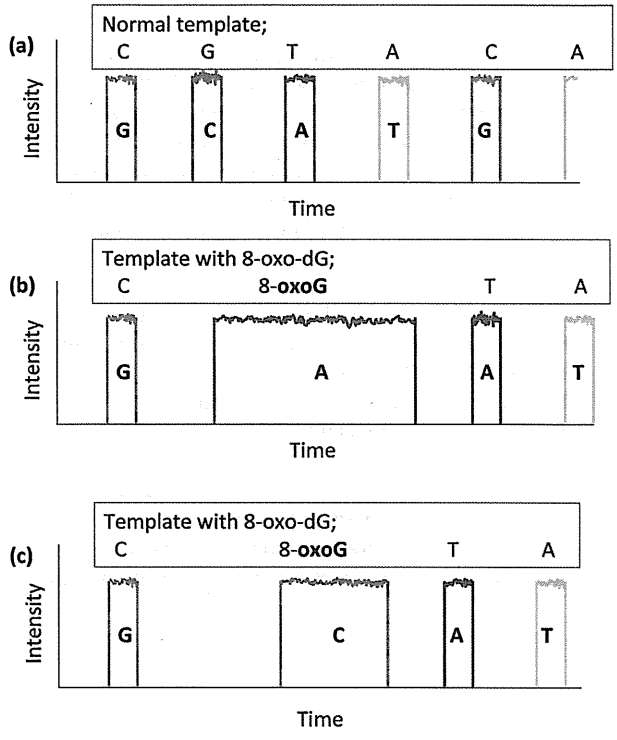

Fig. 3. Expected signal patterns of the SMRT™ DNA sequencer when the template contains 8-oxo-dG. (a) Undamaged DNA was used as a template; sequence reaction proceeds at a speed of tens of bases per second. (b) Template contains 8-oxo-dG; sequence reaction will be retarded opposite 8-oxo-dG. In this case, dA is incorporated opposite 8-oxo-dG. (c) In the case where dC is incorporated opposite 8-oxo-dG, the retardation time will be different from that in the case of dA.

Acknowledgement: This work was supported by KAKENHI (18101003) and Grant-in-aid for scientific research from the Ministry of Health, Labour and Welfare, Japan.

References

1 PACIFIC BIOSCIENCES. Pacific Biosciences Announces Early Access Customers for its Single Molecule Real Time System. (http://pacificbiosciences.com/assets/files/pacbio_early_access_customers_final.pdf). 2010.
2 PACIFIC BIOSCIENCES. Pacific Biosciences Develops Transformative DNA Sequencing Technology. (http://www.pacificbiosciences.com/assets/files/pacbio_technology_backgrounder.pdf). 2010.
3 Fuller CW, Middendorf LR, Benner SA, Church GM, Harris T, Huang X, Jovanovich SB, Nelson JR, Schloss JA, Schwartz DC, Vezenov DV. The challenges of sequencing by synthesis. Nat Biotechnol. 2009; 27:

1013–23.
4 Eid J, Fehr A, Gray J, Luong K, Lyle J, Otto G, Peluso P, Rank D, Baybayan P, Bettman B, Bibillo A, Bjornson K, Chaudhuri B, Christians F, Cicero R, Clark S, Dalal R, Dewinter A, Dixon J, Foquet M, Gaertner A, Hardenbol P, Heiner C, Hester K, Holden D, Kearns G, Kong X, Kuse R, Lacroix Y, Lin S, Lundquist P, Ma C, Marks P, Maxham M, Murphy D, Park I, Pham T, Phillips M, Roy J, Sebra R, Shen G, Sorenson J, Tomaney A, Travers K, Trulson M, Vieceli J, Wegener J, Wu D, Yang A, Zaccarin D, Zhao P, Zhong F, Korlach J, Turner S. Real-time DNA sequencing from single polymerase molecules. Science. 2009; 323: 133–8.
5 Shibutani S, Takeshita M, Grollman AP. Insertion of specific bases during DNA synthesis past the oxidation-damaged base 8-oxodG. Nature. 1991; 349: 431–4.
6 Zhou X, Liberman RG, Skipper PL, Margolin Y, Tannenbaum SR, Dedon PC. Quantification of DNA strand breaks and abasic sites by oxime derivatization and accelerator mass spectrometry: application to gamma-radiation and peroxynitrite. Anal Biochem. 2005; 343: 84–92.
7 Shibutani S, Takeshita M, Grollman AP. Translesional synthesis on DNA templates containing a single abasic site. A mechanistic study of the "A rule". J Biol Chem. 1997; 272: 13916–22.
8 Pang B, Zhou X, Yu H, Dong M, Taghizadeh K, Wishnok JS, Tannenbaum SR, Dedon PC. Lipid peroxidation dominates the chemistry of DNA adduct formation in a mouse model of inflammation. Carcinogenesis. 2007; 28: 1807–13.
9 Yasui M, Suenaga E, Koyama N, Masutani C, Hanaoka F, Gruz P, Shibutani S, Nohmi T, Hayashi M, Honma M. Miscoding properties of 2′-deoxyinosine, a nitric oxide-derived DNA Adduct, during translesion synthesis catalyzed by human DNA polymerases. J Mol Biol. 2008; 377: 1015–23.
10 Yasui M, Suzuki N, Miller H, Matsuda T, Matsui S, Shibutani S. Translesion synthesis past 2′-deoxyxanthosine, a nitric oxide-derived DNA adduct, by mammalian DNA polymerases. J Mol Biol. 2004; 344: 665–74.

Toxicology 274 (2010) 42–48

Contents lists available at ScienceDirect

Toxicology

journal homepage: www.elsevier.com/locate/toxicol

Inhibitory effects of chrysoeriol on DNA adduct formation with benzo[*a*]pyrene in MCF-7 breast cancer cells

Hitomi Takemura[a,b], Haruna Nagayoshi[c], Tomonari Matsuda[c], Hiroyuki Sakakibara[a,d], Maki Morita[d], Asako Matsui[d], Takeshi Ohura[a,d], Kayoko Shimoi[a,d,e,*]

[a] *Institute for Environmental Sciences, University of Shizuoka, 52-1 Yada, Suruga, Shizuoka 422-8526, Japan*
[b] *Department of Health and Nutritional Science, Faculty of Human Health Sciences, Matsumoto University, 2095-1 Niimura, Matsumoto 390-1295, Japan*
[c] *Research Center for Environmental Quality Management, Kyoto University, 1-2 Yumihama, Otsu, Shiga 520-0811, Japan*
[d] *Graduate School of Nutritional and Environmental Sciences, University of Shizuoka, 52-1 Yada, Suruga, Shizuoka 422-8526, Japan*
[e] *Global COE Program, University of Shizuoka, 52-1 Yada, Suruga, Shizuoka 422-8526, Japan*

ARTICLE INFO

Article history:
Received 21 April 2010
Received in revised form 19 May 2010
Accepted 19 May 2010
Available online 27 May 2010

Keywords:
Benzo[*a*]pyrene
Chrysoeriol
Cytochrome P450 1 family
DNA adducts
Liquid chromatography–tandem mass spectrometry

ABSTRACT

Cytochrome P450 (CYP) 1 families including CYP1A1, 1A2 and 1B1 are well known to be deeply involved in the initiation of several cancers, due to the fact that they activate environmental pro-carcinogens to form ultimate carcinogens. Benzo[*a*]pyrene (BaP) is one of the major classes of prototypical pro-carcinogen. It is activated by the CYP1 family to its ultimate carcinogenic forms, mainly BaP-7,8-diol-9,10-epoxide (BPDE), and it forms adducts with DNA. This has been recognized to be a major initiation pathway for cancer. Our previous study demonstrated that chrysoeriol, which is a dietary methoxyflavonoid, selectively inhibited CYP1B1 enzymatic activity and might protect the CYP1B1 related-diseases such as breast cancer. In the present study, we further examined the effects of chrysoeriol on the other initiation pathway of cancer relating to the CYP1 family with BaP in human breast cancer MCF-7 cells. The effects of chrysoeriol on the formation of BPDE-DNA adducts were analyzed specifically using the liquid chromatography–tandem mass spectrometry (LC–MS/MS) method. When MCF-7 cells were incubated with 2 μM BaP for 24 h, three types of BPDE-dG adducts, especially (+)-*trans*-BPDE-dG as the dominant adduct, were detected. Co-treatment of MCF-7 cells with 10 μM chrysoeriol and BaP remarkably reduced (+)-*trans*-BPDE-dG formation. Chrysoeriol (1–10 μM) dose-dependently inhibited both EROD activity and the gene expressions of CYP1A1, 1B1 and 1A2 stimulated by treatment with BaP. In addition, the same amounts of chrysoeriol significantly inhibited the binding of BaP to the aryl hydrocarbon receptor (AhR), which is the key factor concerning the induction of the CYP1 families. In conclusion, our results clearly indicate that chrysoeriol inhibited the formation of BPDE-DNA adducts *via* regulation of the AhR pathway stimulated by BaP. As a consequence chrysoeriol may be involved in the chemoprevention of environmental pro-carcinogens such as BaP.

1. Introduction

Polycyclic aromatic hydrocarbons (PAHs) are an environmentally ubiquitous class of compounds that are formed during incomplete combustion of organic substances. Several PAHs have been classified as probable human carcinogens (Boffetta et al., 1997; Shimada, 2006). Animal studies have provided further support for the role of PAHs as mammary carcinogens (Cavalieri et al., 1991; el-Bayoumy et al., 1995; Hecht, 2002). When PAHs are absorbed into the body they reach some organs, such as the liver, lung and mammary glands. After activation in tissues by metabolizing enzymes such as the cytochrome P450 (CYP) 1 family, PAHs reacts with DNA and forms adducts, the so-called PAH-DNA adducts. This step has been recognized to be a major initiation pathway for carcinogenesis induced by PAHs (Levin et al., 1977; Conney, 1982; Pelkonen and Nebert, 1982). On the contrary, PAHs themselves are basically inactive. Therefore, intact PAHs and activated PAHs are termed as pro-carcinogens and ultimate carcinogens, respectively. The Long Island Breast Cancer Study Project (LIBCSP), a large population-based case–control study, reported that blood levels of PAH-DNA adduct were associated with a modest 29–35% elevation in breast cancer risk among women (Gammon et al., 2004).

Abbreviations: AhR, aryl hydrocarbon receptor; BaP, benzo[*a*]pyrene; BPDE, 7,8-dihydroxy-9,10-epoxy-7,8,9,10-tetrahydrobenzo[*a*]pyrene; CYP, cytochrome P450; EROD, 7-ethoxyresorufin-*O*-deethylation; LC–MS/MS, liquid chromatography–tandem mass spectrometry.

* Corresponding author at: Institute for Environmental Sciences, University of Shizuoka, 52-1 Yada, Shizuoka 422-8526, Japan. Tel.: +81 54 264 5787; fax: +81 54 264 5787.
E-mail address: shimoi@u-shizuoka-ken.ac.jp (K. Shimoi).

0300-483X/$ – see front matter © 2010 Elsevier Ireland Ltd. All rights reserved.
doi:10.1016/j.tox.2010.05.009

Benzo[*a*]pyrene (BaP), a typical pro-carcinogenic PAH, is a ubiquitous environmental pollutant and is also present in tobacco smoke, coal tar, automobile exhaust emissions and charred food. It is categorized in Group 1 (carcinogenic to humans) in the list published by the International Agency for Research on Cancer (see: http://monographs.iarc.fr/ENG/Classification/index.php). However, BaP itself has no carcinogenic effect. When BaP reaches the target organ it activates the aryl hydrocarbon receptor (AhR), which forms an active transcription factor heterodimer with the AhR nuclear translocator (ARNT), and consequently induces the CYP1 family, such as CYP1A1, 1A2 and 1B1 (Nebert et al., 2000). Subsequently, BaP is metabolized to its ultimate carcinogenic forms, mainly 7,8-dihydroxy-9,10-epoxy-7,8,9,10-tetrahydrobenzo[*a*]pyrene (BPDE), by the CYP1 family induced by BaP itself. BPDE is a biologically active metabolite and immediately makes several kinds of adducts with DNA (Conney, 1982). Some researchers have reported that BPDE-DNA adduct formation induces DNA miss-replication and mutation, and as a consequence initiates the carcinogenic process (Kapitulnik et al., 1977; Shimada et al., 2001). Actually, animal studies in rats treated with orally administered BaP confirm its mammary carcinogenicity (el-Bayoumy et al., 1995). These findings suggest that protection of BPDE-DNA adduct formation will lead to anticarcinogenesis.

BPDE has been reported to form the stereoselective metabolite, 7β,8α-dihydroxy-9α,10α-epoxy-7,8,9,10-tetrahydrobenzo[*a*]pyrene [(±)-*anti*-BPDE]. It has also been reported to react covalently with the guanine residues of DNA to form N^2-deoxyguanosine (dG) adducts (Grollman and Shibutani, 1994; Suzuki et al., 2002), adopting either trans and cis stereoisomeric configurations, i.e., (±)-*trans*-BPDE-dG and (±)-*cis*-BPDE-dG. Striking differences in the biological activities of these four stereoisomeric BPDE-dG adducts have been reported (Sundberg et al., 2002; Dong et al., 2004; Ruan et al., 2007). The (+)-*anti*-BPDE is the most tumorigenic adduct, causing pulmonary adenomas in mice (Buening et al., 1978; Kapitulnik et al., 1978; Chang et al., 1987). The (+)-*trans* type of adduct is reported to be the most abundant BPDE-dG adduct among the four stereoisomeric dG adducts, and thus is the most influential adduct for carcinogenic potency as compared with the other adducts (Ruan et al., 2007; Feng et al., 2009). Therefore, it is important to qualitatively and quantitatively evaluate stereoisomeric BPDE-dG adducts in DNA to understand the mutagenic and carcinogenic effects of BaP.

A number of methods have been developed for the characterization and/or detection of BPDE-DNA adducts. A ^{32}P-postlabelling and spectroscopic analysis have been classically used as sensitive methods for the determination of BPDE-DNA adducts. However, few methods demonstrate the capability of resolving the stereoisomers of BPDE-DNA adducts. Recently, liquid chromatography–tandem mass spectrometry (LC–MS/MS) methods have been described for the detection and quantitation of the four stereoisomeric BPDE-dG adducts (Feng et al., 2008), and have been reported to be a useful method for detection of BaP-derived DNA adducts in human lung cells (Feng et al., 2009). Therefore, the LC–MS/MS technique might offer a precise method to evaluate BPDE-dG adduct formation.

In an in vitro study we previously investigated the effects of chrysoeriol (3′-methoxy-4′,5,7-trihydroxyflavone), which is a methoxy flavone that exists in botanical foods (Choi et al., 2005; Khan and Gilani, 2006; Lin et al., 2007; Snijman et al., 2007), on the metabolism of endogenous estrogen and 17β-estradiol (E_2), stimulated by recombinant human CYP1A1 and CYP1B1 (Takemura et al., 2010). Like BaP, E_2 is a pro-carcinogen and is metabolized mainly by CYP1B1 to its ultimate carcinogen, 4-hydroxyl-E_2. Chrysoeriol selectively inhibits human recombinant CYP1B1-mediated 7-ethoxyresorufin-*O*-deethylation (EROD) activity five times more effectively than CYP1A1-mediated activity at a concentration of 0.1 μM. Additionally, chrysoeriol significantly inhibits the formation of 4-methoxy-E_2, which is a metabolite of 4-hydroxy-E_2, in MCF-7 cells, one of the major human breast cancer cell lines. These findings led us to hypothesize that chrysoeriol might have chemopreventive effects against environmental pro-carcinogens, such as BaP activated by the CYP1 family.

In the present study, we investigated the inhibitory effects of chrysoeriol on BaP-induced DNA adduct formation in human MCF-7 breast cancer cells using LC–MS/MS analysis. Additionally, in order to clarify the inhibition mechanism, we evaluated the effects of chrysoeriol on BaP-induced CYP1s activations, and CYP1 mRNA induction in MCF-7 cells. Furthermore, we verified the antagonistic activity of chrysoeriol against BaP-induced activation of AhR using an AhR-based bioassay. This is the first report concerning the inhibitory effects of chrysoeriol on the formation of specific stereoisomeric BPDE-dG adducts using the LC–MS/MS method.

2. Materials and methods

2.1. Chemicals

HPLC grade chrysoeriol was purchased from Extrasynthèse (Genay, France). Chrysoeriol was dissolved in dimethyl sulfoxide (DMSO) at a concentration 20 mM and stored at −20 °C in the dark for up to 3 months. Ethoxyresorufin, 4-hydroxycoumarin and RNase T1 were obtained from Sigma Chemical Co. (St. Louis, MO, USA). RNase A and protease K were sourced from Qiagen Inc. (Valencia, CA, USA). [U-$^{15}N_5$] 2′-deoxyguanosine was purchased from Cambridge Isotope Laboratories, Inc. (Andover, MA, USA). (±)BPDE was a kind gift from Dr. Nicholas E. Geacintov of New York University (New York, NY, USA). [U-$^{15}N_5$]-BPDE-dG as an internal standard for LC–MS/MS was synthesized by mixing (±)BPDE and [U-$^{15}N_5$] 2′-deoxyguanosine, and fractionated using HPLC according to the method reported by Singh et al. (Singh et al., 2006). The oligodeoxynucleotide containing a single (+)-*trans*-BPDE-dG was provided from Dr. Shibutani, State University of New York at Stony Brook (Terashima et al., 2002). The Ah-immunoassay (Ah-I) was obtained from Entest Japan, Inc. (Tokyo, Japan). All the other chemicals and reagents used in the study were of the highest grade available.

2.2. Cell culture

Human breast cancer MCF-7 cells that were kindly provided by Dr. H. Hagenmaier (University of Tuebingen, Baden-Wuerttemberg, Germany) were cultured in Dulbecco's modified Eagle medium (DMEM) supplemented with 10% fetal bovine serum, 0.1 mg/mL penicillin and 0.1 mg/mL streptomycin at 37 °C under 5% CO_2. We examined ahead effects of BaP and chrysoeriol on cell viability, and obtained the results that existence of BaP and/or chrysoeriol were not exert any affects on the cell survivals up to 2 and 10 μM, respectively, until 48 h of incubations (data not shown).

2.3. DNA isolation

When cells were sub-confluent in Ø100 mm dishes, the medium was changed to estrogen free DMEM including 2 μM BaP and/or 5–10 μM chrysoeriol. Dimethyl sulfoxide (DMSO; 0.1% of final volume) was used as a vehicle control in the experiment. After incubation for 24 h, cells were replaced from dishes and immediately progressed to DNA isolation as described below. The NaI method was used for DNA isolation from cells as previously described with slight modifications (Ravanat et al., 2002). Briefly, the cells were homogenized in 1.0 mL of lysis buffer A at pH 7.5 (320 mM sucrose, 5 mM $MgCl_2$, 10 mM Tris and 0.1 mM desferrioxamine) with 1% Triton X-100. The nuclei were collected by centrifugation at 1500 × *g* for 5 min at 4 °C. The nuclear pellet was resuspended in 200 μL buffer B at pH 8.0 (10 mM Tris, 5 mM EDTA and 0.15 mM desferrioxamine) and was then mixed with 10% SDS. To the solution were added 8 μL of RNase A (1 mg/mL) and 16 μL of RNase T1 (1 U/μL in RNase buffer; 10 mM Tris, 1 mM EDTA and 2.5 mM desferrioxamine at pH 7.4) and were incubated at 50 °C for 15 min. Then, the samples were treated with 40 μL of protease K (20 mg/mL in distilled water) and incubated at 55 °C for 1 h. Samples were centrifuged at 5000 × *g* for 5 min at room temperature. The supernatant was collected and mixed with 400 μL of the NaI solution (7.6 M NaI, 40 mM Tris, 20 mM EDTA and 0.3 mM desferrioxamine at pH 8.0) and 670 μL of 2-propanol was added. DNA precipitation was achieved by gently inverting the tube several times. After centrifugation at 5000 × *g* for 15 min at 4 °C, DNA was washed twice with 1 mL of 40% 2-propanol. The DNA pellet was washed again using 1 mL of 70% ethanol. Finally, DNA was recovered by centrifugation and dissolved in distilled water. The DNA concentrations were determined by measuring the absorbance at 260 nm.

2.4. DNA digestion

Fifty microgram aliquots of DNA were digested into their constituent 2′-deoxyribonucleoside units by the addition of 15 μL of 17 mM succinate and 8 mM

$CaCl_2$ buffer (pH 6.0) that contained micrococcal nuclease (7.5 U), spleen phosphodiesterase (0.025 U) and [U-$^{15}N_5$]-BPDE-dG as internal standards. The solutions were mixed and incubated for 3 h at 37 °C, then which alkaline phosphatase (3 U), 10 μL of 0.5 M Tris–HCl (pH 8.5), 5 μL of 20 mM $ZnSO_4$ and 67 μL of distilled water were added, and incubated for further 3 h at 37 °C. The digested sample was extracted twice with methanol. The methanol fractions were evaporated to dryness, resuspended in 50 μL of 30% DMSO solution and subjected to LC–MS/MS.

2.5. LC–MS/MS analysis of BPDE-dG

LC–MS/MS analysis was performed using a Shimadzu LC system (Shimadzu Co., Kyoto, Japan) interfaced with a Waters Micromass Quattro Ultima triple stage quadrupole mass spectrometer (Waters, Manchester, UK). Each sample was separated on a Shim-pack XR-ODS column (Ø3.0 mm × 75 mm, 2.2 μm, Shimadzu Co., Kyoto, Japan) at a flow rate of 0.2 ml/min. The elution was carried out using 55% methanol isocratic for 20 min. The multiple reaction monitoring (MRM) mode was used to monitor *m/z* 575 > 459 (for the internal standard) and *m/z* 570 > 454 (for BPDE-dG). The standard curve of (+)-*trans*-BPDE-dG was obtained by digesting 50 μg of calf thymus DNA spiked with various amounts of 24-mer oligonucleotide containing single (+)-*trans*-BPDE-dG and [U-$^{15}N_5$]-BPDE-dG.

2.6. EROD assay in MCF-7 cells

The EROD assay was employed as a method for the evaluation of CYP1 activity in cells with slight modifications (Ciolino and Yeh, 1999). In brief, subconfluent MCF-7 cells in 24-well plates were treated with 1 mL of phenol red-free DMEM containing 2 μM BaP and/or 0.5–10 μM chrysoeriol. DMSO was used as a vehicle control in the experiment. After incubation for 48 h, the medium was removed and the wells were washed twice with phenol red-free DMEM, and the media were replaced with 1.8 mL of medium containing 2.5 μM ethoxyresorufin and 0.2 mM dicumarol. It was then incubated at 37 °C for 20 min. The formation of resorufin was determined fluorometrically (530 nm excitation and 590 nm emission) with a spectrofluorometer (Thermo Fisher Scientific Inc., Worcester, MA, USA).

2.7. Real-time quantitative RT-PCR analysis

Total RNA was isolated from MCF-7 cells treated with 2 μM BaP and/or 1–10 μM chrysoeriol for 12 h using the RNA Protect Cell Reagent (Qiagen Inc., Valencia, CA, USA) and the RNeasy Plus Mini Kit (Qiagen Inc.) according to the protocol included. DMSO was used as a vehicle control in the experiment. Following isolation, RNA quantity, purity and concentration were determined using a Gene Quant pro spectrophotometer (Amersham Biosciences, Foster City, CA, USA).

The RNA sample (300 ng) was added to 20 μL of reaction mixture containing random hexamers, MuLv Reverse Transcriptase, RNase inhibitors, 25 mM $MgCl_2$, 10 × PCR Buffer II (Applied Biosystems, Foster City, CA, USA), and 10 mM dNTP mix (Promega Co., Madison, WI, USA). Synthesis of cDNA was performed at 42 °C for 60 min and the reverse transcription reaction was stopped by heating to 95 °C for 7 min, followed by chilling on ice. The cDNA was stored at −20 °C until further use. A total of 2 μL of cDNA was added to the 18 μL of PCR mixture containing 10 μL Taq Man Gene Expression Master Mix (Applied Biosystems), 6 μL distilled water DNase RNase Free (Invitrogen Co., Carlsbad, CA, USA), 1 μL house-keeping gene solution (glyceraldehyde-3-phosphate dehydrogenase; *GAPDH*), and 1 μL individual target gene expression reagents (cytochrome P450, family 1, subfamily A, polypeptide 1 (*CYP1A1*), Assay ID, Hs00153120_m1; cytochrome P450, family 1, subfamily A, polypeptide 2 (*CYP1A2*), Assay ID, Hs01070374_m1; cytochrome P450, family 1, subfamily B, polypeptide 1 (*CYP1B1*), Assay ID, Hs00164383_m1). Real-time quantitative PCR was performed on a 7500 Real-Time PCR System (Applied Biosystems) as described previously (Ohura et al., 2010). The samples were amplified by incubation for 2 min at 50 °C, then 10 min at 95 °C, followed by 40 cycles at 95 °C for 15 s and 60 °C for 1 min. The relative expression level of the target gene product was calculated by the comparative automatic threshold cycles method, using the housekeeping gene, *GAPDH*, as a calibrator. The threshold cycle values for each sample were set up at constant 0.2. The relative differences in expression between groups were expressed using cycle time values and the relative differences between groups were expressed as relative increases, setting the control as 100%.

2.8. AhR antagonistic activity in Ah-immunoassay

To evaluate AhR-based activities, Ah-Immunoassay (Ah-I) was carried out as described previously (Amakura et al., 2003). The Ah-I method is a receptor-binding assay using cytosol containing AhR extracted from mammalian liver cells and immunologically measures the dioxin level utilizing an antigen–antibody reaction. Briefly, the cytosol (200 μL) was added to chrysoeriol, or to DMSO alone as the control. The mixture was preincubated for 20 min and then incubated with 0.1 μM BaP for 2 h at 30 °C. After incubation, the formation of the AhR-BaP complex was determined using an Ah-I kit. AhR activity was calculated as $\{1-[(A-B)-(C-D)]/(A-B)\} \times 100$, where *A* is the absorbance of the control with BaP added, *B* is the absorbance of the control with DMSO added, *C* is the absorbance of chrysoeriol with BaP added, and *D* is the absorbance of chrysoeriol with DMSO added. All experiments were carried out in triplicate. The values obtained with BaP alone were considered as 100% of the control value.

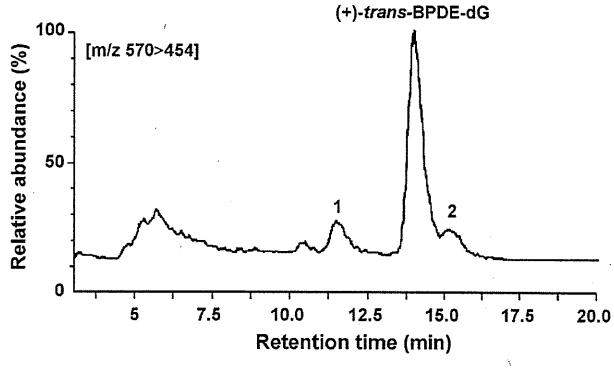

Fig. 1. Typical HPLC chromatogram of stereoisomers of BPDE-dG adducts formed in MCF-7 cells treated with 2 μM BaP. Peak 1 and Peak 2 might be (+)-*cis*-BPDE-dG and *syn*-BPDE-dG, respectively, as referred to in previous reports (Ruan et al., 2007; Feng et al., 2008, 2009).

2.9. Statistical analysis

Results were expressed as the mean ± standard deviation (SD) for experiments performed in at least triplicate. Statistical significance of differences was evaluated using Tukey's multiple comparison tests using Pharmaco Analysis II Software.

3. Results

3.1. Effects of chrysoeriol on BPDE-dG adducts formation in MCF-7 cells

The three BPDE-dG isomers were detected in BaP-treated cells on LC–MS/MS analysis (Fig. 1). Predominant peak elucidated at 14.0 min of retention time was identified as (+)-*anti-trans*-BPDE-N^2-dG [(+)-*trans*-BPDE-dG] because its retention time was confirmed to that of the standard compound used in this study. The other peaks could not be identified exactly, but it was considered that peak 1 might be (+)-*anti-cis*-BPDE-N^2-dG [(+)-*cis*-BPDE-dG], and peak 2 might be *syn*-BPDE-N^2-dG [*syn*-BPDE-dG] as referred to in the report by Feng et al. (2009). The average abundance of these three adducts in BaP-treated cells were 4.29 ± 0.62, 41.46 ± 8.63, 2.37 ± 0.87 adducts/10^7 bases, respectively. Co-treatments of 5 and 10 μM of chrysoeriol with BaP dose-dependently inhibited the formation of (+)-*cis*-BPDE-dG and (+)-*trans*-BPDE-dG, as compared with BaP in cells without chrysoeriol treatment, respectively (Fig. 2). At higher concentrations (10 μM) both formations were decreased significantly by 21% and 65%, respectively. On the other hand, 5 and 10 μM of chrysoeriol had no effect on the formation of *syn*-BPDE-dG as minor adducts. Consequently, the sum total of the formation of three BPDE-dG adducts was diminished dose-dependently as compared with BaP in cells without chrysoeriol treatment (Fig. 2).

3.2. Effects of chrysoeriol on EROD activity of BaP-treated MCF-7 cells

EROD activity after exposure to 2 μM BaP for 48 h was significantly increased and was 3.9 ± 0.14-fold higher than the vehicle control (Fig. 3). Both 5 and 10 μM of chrysoeriol significantly and dose-dependently inhibited this increase in EROD activity due to treatment with BaP, 2.1 ± 0.14- and 1.3 ± 0.05-fold than vehicle control ($P < 0.01$ *versus* group treated with BaP), respectively. On the other hand, less than 1 μM of chrysoeriol did not induce any inhibitory effect.

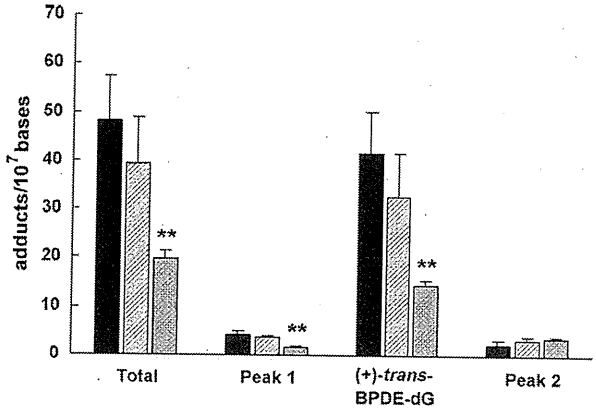

Fig. 2. Inhibitory effects of chrysoeriol on BPDE-dG adduct formation in MCF-7 cells. Each adduct corresponded to the chromatogram in Fig. 1. Data are presented as the mean ± SD (n = 3). Statistical analysis for multiple comparison was performed using Tukey's test (**P < 0.01 *versus* group treated with BaP only). Closed bar, BaP treatment without chrysoeriol; slash lined bar, BaP and 5 μM chrysoeriol treatment; dotted bar, BaP and 10 μM chrysoeriol treatment.

3.3. *Effects of chrysoeriol on CYP1 mRNA expression of BaP-treated MCF-7 cells*

BaP treatment (2 μM) of MCF-7 cells for 12 h resulted in significant increases in the CYP1A1, CYP1A2 and CYP1B1 mRNA levels which were approximately 80 ± 6.6-, 17 ± 3.0- and 5.8 ± 0.81-fold higher than the vehicle control, respectively (Fig. 4). In the presence of chrysoeriol, all three CYP1 mRNA levels were inhibited in a dose-dependent manner. In particular, the expressions of CYP1A1 and 1A2 genes were significantly inhibited even at 1 μM of chrysoeriol (P < 0.05), 5, 10 μM of chrysoeriol (P < 0.01), respectively.

3.4. *AhR antagonistic activity of chrysoeriol*

We used the AhR-based bioassay in order to evaluate the influence of chrysoeriol on the AhR pathway stimulated by BaP. As shown in Fig. 5, chrysoeriol exhibited appreciable dose-dependent inhibition, ranging from 0.1 to 10 μM when activated by 0.1 μM of BaP treatment in this assay system. The inhibitory effects of chrysoeriol at 0.1, 1 and 10 μM were significant, 56.6 ± 9.1%, 37.3 ± 6.3% and 35.6 ± 2.8% (P < 0.01), respectively. On the other hand, chrysoeriol itself did not have any effects on AhR activation at concentrations of up to 10 μM (data not shown).

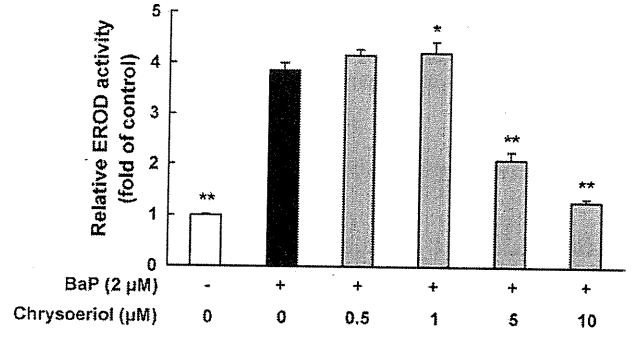

Fig. 3. Inhibitory effects of chrysoeriol on BaP-induced EROD activity in MCF-7 cells. Data are presented as the mean ± SD (n = 4). Statistical analysis for multiple comparison was performed using Tukey's test (*P < 0.05, **P < 0.01 *versus* control group treated with BaP without chrysoeriol).

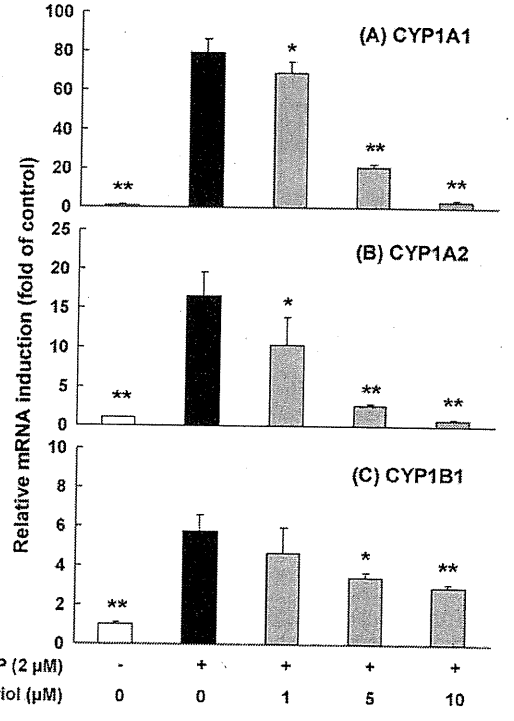

Fig. 4. Inhibitory effects of chrysoeriol on BaP-induced CYP1A1, CYP1A2 and CYP1B1 expression in MCF-7 cells. Data are presented as the mean ± SD (n = 3). Statistical analysis for multiple comparison was performed using Tukey's test (*P < 0.05, **P < 0.01 *versus* control group treated with BaP without chrysoeriol).

4. Discussion

In the present study, we demonstrated that chrysoeriol had a preventive effect on stereoisomeric BPDE-dG formation in human MCF-7 breast cancer cells treated with BaP using the LC–MS/MS technique. When MCF-7 cells were incubated with 2 μM of BaP for 24 h, three types of BPDE-dG adducts were detected. Predominant peak was identified as (+)-*trans*-BPDE-dG, because its retention time was confirmed to that of the standard compound used in our study. The (+)-*trans*-BPDE-dG was the dominant adduct in MCF-7 cells treated with BaP. This finding was consistent with two other studies which involved human bronchoalveolar H385 cells exposed to 2 μM BaP or 2 μM (±)-BaP-7,8-dihydroxydiol (Ruan et al., 2007) and human lung A549 cells exposed to 5 μM

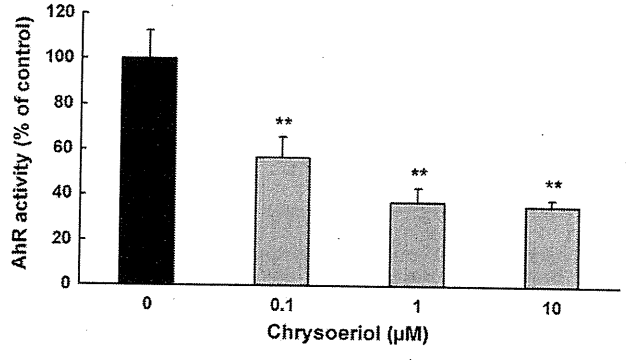

Fig. 5. Inhibitory effects of chrysoeriol on the AhR activation induced by BaP. The values obtained with BaP alone were considered to be 100% of the control value. Data are presented as the mean ± SD (n = 3). Statistical analysis for multiple comparison was performed using Tukey's test (**P < 0.01 *versus* vehicle controls treated with BaP alone).

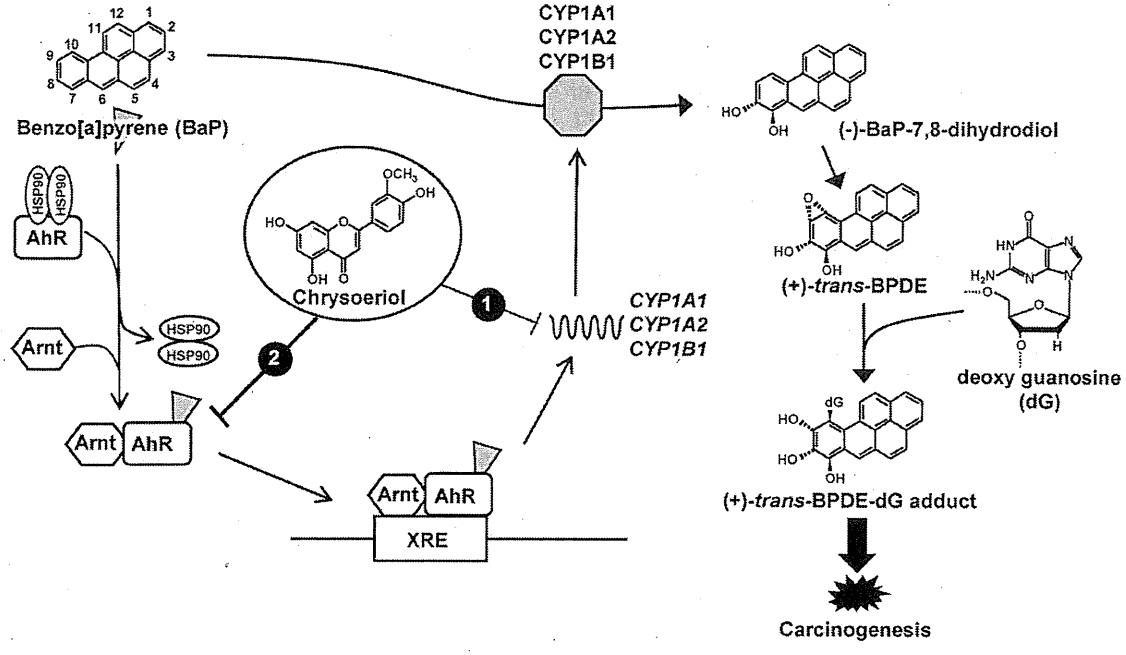

Fig. 6. Putative inhibitory mechanisms of chrysoeriol on BPDE-dG adduct formations in MCF-7 cells. HSP90, heat shock protein 90; AhR, arylhydrocarbon receptor; Arnt, AhR nuclear translocator; XRE, xenobiotic responsive element; BPDE, BaP-7,8-diol-9,10-epoxide (BPDE).

BaP (Feng et al., 2009). The (+)-*trans*-BPDE-dG adducts from (−)-BaP-7,8-dihydrodiol were detected in approximately twice the amount observed for (±)-BaP-7,8-dihydroxydiol-exposed H385 cells. In contrast, (+)-*trans*-BPDE-dG was not observed in (+)-BaP-7,8-dihydroxydiol-exposed cells. Therefore, the major adduct was (+)-*trans*-BPDE-dG, which means that the (−)-BaP-7,8-dihydrodiol-derived metabolite (+)-*anti*-BPDE was mainly responsible for DNA adduct formation (Cheng et al., 1989; Geacintov et al., 1997; Ruan et al., 2007). Three BPDE-dG adducts, in which (+)-*trans*-BPDE-dG was dominant and (+)-*cis*-BPDE-dG and *syn*-BPDE-dG were minors, were detected in A549 cells and H358 cells treated with BaP (Ruan et al., 2007; Feng et al., 2009), although four adducts appeared in A549 cells treated with BPDE (Feng et al., 2009). Hence, in common with human A549 lung cells and human bronchoalveolar H358 cells our results indicated that human MCF-7 breast cancer cells treated with BaP also generated three BPDE-dG adducts. Additionally, with the exception of (+)-*trans*-BPDE-dG, other peaks in our results could not be precisely identified. However, it was considered that peak 1 might be (+)-*cis*-BPDE-dG, and peak 2 might be *syn*-BPDE-dG, as referred to in previous reports (Ruan et al., 2007; Feng et al., 2008, 2009). Further studies are needed for the identification of these two adducts.

Co-treatment involving 1–10 μM chrysoeriol in combination with BaP inhibited the sum total formation of BPDE-dG adducts in MCF-7 cells in a dose-dependant manner (Fig. 2). In particular, among the three adducts (+)-*trans*-BPDE-dG formation was incredibly diminished in the presence of chrysoeriol. (+)-*trans*-BPDE-dG is considered to be highly mutagenic in mammalian cells (Fernandes et al., 1998; Huang et al., 2003) and to be responsible for the observed tumorigenic effects in mouse skin (Levin et al., 1977) and mouse lung (Buening et al., 1978). Therefore, our results clearly indicate that chrysoeriol might be an effective food ingredient that could prevent DNA adduct formation with pro-carcinogens such as BaP. Chrysoeriol also inhibited the formation of Peak 1 ((+)-*cis*-BPDE-dG generated in MCF-7 cells by treatment with BaP) but did not inhibit the formation of Peak 2 (*syn*-BPDE-dG). Human breast cells are also known to express the other CYP families, such as CYP2C6, 2D6, 2E1, 3A4 and 3A5 (Williams and Phillips, 2000). CYP3A5 catalyzes the metabolism of (−)-BaP-7,8-dihydrodiol to (+)-*anti*-BPDE (Roberts-Thomson et al., 1993), whereas little is known about the stereoselective metabolism of BaP-7,8-dihydrodiol by the other CYPs. *syn*-BPDE-dG might be produced by the other CYPs that are present in breast cells.

We further extended the investigation in order to elucidate the mechanisms involved in the prevention of BPDE-dG formation by chrysoeriol. BaP itself is not a mutagenic or carcinogenic compound until bioactivated by xenobiotic-metabolizing enzymes such as those in the CYP1 family and epoxide hydrolase (Conney, 1982; Pelkonen and Nebert, 1982; Hecht, 2002; Shimada, 2006). Additionally, of special note in relation to the CYP1 family and BaP is that BaP itself induces CYP1s (Nebert et al., 2000, 2004). Chrysoeriol clearly inhibited BaP-induced EROD activity in MCF-7 cells by roughly the same magnitude as observed in the experiment above (Fig. 3). Moreover, chrysoeriol significantly inhibited the gene expression of individual CYP1A1, 1A2 and 1B1 mRNA stimulated by BaP in MCF-7 cells (Fig. 4). It is well recognized that the expression of the CYP1 family genes are regulated by AhR, a ligand activated transcription factor (Whitlock, 1999; Nebert et al., 2004). Hence, in the final part of our study, using an AhR-based bioassay, we evaluated the antagonistic activity of chrysoeriol against BaP-induced activation of AhR. We found that BaP powerfully stimulated AhR activity, but the co-existence of chrysoeriol diminished this stimulation in a dose-dependent manner (Fig. 5). Many researchers have demonstrated the AhR antagonistic activities of substituted 3′-methoxyflavones in MCF-7 cells (Lu et al., 1995), human MCF-10A breast epithelial cells (Reiners et al., 1998) and mouse Hepa-1c1c7 hepatoma cells (Gasiewicz et al., 1996; Henry et al., 1999). In addition, 3′,4′-methoxyflavone inhibited both AhR-mediated CYP1A1 induction and antiestrogenic activity in both MCF-7 and T47D breast cancer cell lines by blocking the transformation of the cytosolic AhR complex and the formation of the nuclear AhR complex (Lee and Safe, 2000). In the present study, chrysoeriol exhibited inhibitory effects on the formation of BPDE-dG adducts *via* the regulation of the AhR pathway, including activation of the CYP1 family stimulated by BaP. This finding indicated that 3′-methoxy-substituted flavones such as chrysoeriol might be potent AhR antagonists in breast cancer cells.

In conclusion, the present study is the first to report to demonstrate that chrysoeriol has preventive effects on BPDE-dG adduct formation in MCF-7 cells treated with BaP and evaluated using the LC–MS/MS technique. As shown in Fig. 6, pro-carcinogen BaP activates AhR pathway, and induces CYP1A1, 1A2 and 1B1 expression. Furthermore, BaP itself is metabolized to BPDE, mainly (+)-*trans*-BPDE, by induced CYP1s. Following, BPDE reacts with deoxyguanosine (dG), and forms BPDE-dG adducts, in which (+)-*trans*-BPDE-dG is dominant. In this study, the formation of (+)-*trans*-BPDE-dG was dramatically diminished by a 10 μM concentration of chrysoeriol. One of the inhibitory mechanisms is considered as inhibition of CYP1s' gene expressions (Fig. 6, pathway 1), *via* blocking the formation of the AhR-BaP complex (Fig. 6, pathway 2). As a consequence, chrysoeriol may be involved in the chemoprevention of environmental pro-carcinogens such as BaP.

Conflict of interest statement

The authors declare that there are no conflicts of interest.

Acknowledgments

This work was supported partly by a Grant-in-Aid for Young Scientists (B) (20700601) from the Ministry of Education, Culture, Sports, Science and Technology of Japan. Additional funding was provided by the Global COE Program, the Center of Excellence for Innovation in Human Health Sciences, from the Ministry of Education, Science, Sports and Culture of Japan.

References

Amakura, Y., Tsutsumi, T., Sasaki, K., Yoshida, T., Maitani, T., 2003. Screening of the inhibitory effect of vegetable constituents on the aryl hydrocarbon receptor-mediated activity induced by 2,3,7,8-tetrachlorodibenzo-p-dioxin. Biol. Pharm. Bull. 26, 1754–1760.

Boffetta, P., Jourenkova, N., Gustavsson, P., 1997. Cancer risk from occupational and environmental exposure to polycyclic aromatic hydrocarbons. Cancer Causes Control 8, 444–472.

Buening, M.K., Wislocki, P.G., Levin, W., Yagi, H., Thakker, D.R., Akagi, H., Koreeda, M., Jerina, D.M., Conney, A.H., 1978. Tumorigenicity of the optical enantiomers of the diastereomeric benzo[a]pyrene 7,8-diol-9,10-epoxides in newborn mice: exceptional activity of (+)-7beta,8alpha-dihydroxy-9alpha,10alpha-epoxy-7,8,9,10-tetrahydrobenzo[a]pyrene. Proc. Natl. Acad. Sci. U.S.A. 75, 5358–5361.

Cavalieri, E.L., Higginbotham, S., RamaKrishna, N.V., Devanesan, P.D., Todorovic, R., Rogan, E.G., Salmasi, S., 1991. Comparative dose–response tumorigenicity studies of dibenzo[alpha,l]pyrene versus 7,12-dimethylbenz[a]pha]anthracene, benzo[alpha]pyrene and two dibenzo[alpha,l]pyrene dihydrodiols in mouse skin and rat mammary gland. Carcinogenesis 12, 1939–1944.

Chang, R.L., Wood, A.W., Conney, A.H., Yagi, H., Sayer, J.M., Thakker, D.R., Jerina, D.M., Levin, W., 1987. Role of diaxial versus diequatorial hydroxyl groups in the tumorigenic activity of a benzo[a]pyrene bay-region diol epoxide. Proc. Natl. Acad. Sci. U.S.A. 84, 8633–8636.

Cheng, S.C., Hilton, B.D., Roman, J.M., Dipple, A., 1989. DNA adducts from carcinogenic and noncarcinogenic enantiomers of benzo[a]pyrene dihydrodiol epoxide. Chem. Res. Toxicol. 2, 334–340.

Choi, D.Y., Lee, J.Y., Kim, M.R., Woo, E.R., Kim, Y.G., Kang, K.W., 2005. Chrysoeriol potently inhibits the induction of nitric oxide synthase by blocking AP-1 activation. J. Biomed. Sci. 12, 949–959.

Ciolino, H.P., Yeh, G.C., 1999. Inhibition of aryl hydrocarbon-induced cytochrome P-450 1A1 enzyme activity and CYP1A1 expression by resveratrol. Mol. Pharmacol. 56, 760–767.

Conney, A.H., 1982. Induction of microsomal enzymes by foreign chemicals and carcinogenesis by polycyclic aromatic hydrocarbons: G. H. A. Clowes Memorial Lecture. Cancer Res. 42, 4875–4917.

Dong, H., Bonala, R.R., Suzuki, N., Johnson, F., Grollman, A.P., Shibutani, S., 2004. Mutagenic potential of benzo[a]pyrene-derived DNA adducts positioned in codon 273 of the human P53 gene. Biochemistry (Mosc.) 43, 15922–15928.

el-Bayoumy, K., Chae, Y.H., Upadhyaya, P., Rivenson, A., Kurtzke, C., Reddy, B., Hecht, S.S., 1995. Comparative tumorigenicity of benzo[a]pyrene, 1-nitropyrene and 2-amino-1-methyl-6-phenylimidazo[4,5-b]pyridine administered by gavage to female CD rats. Carcinogenesis 16, 431–434.

Feng, F., Wang, X., Yuan, H., Wang, H., 2009. Ultra-performance liquid chromatography–tandem mass spectrometry for rapid and highly sensitive analysis of stereoisomers of benzo[a]pyrene diol epoxide-DNA adducts. J. Chromatogr. B: Anal. Technol. Biomed. Life Sci. 877, 2104–2112.

Feng, F., Yin, J., Song, M., Wang, H., 2008. Preparation, identification and analysis of stereoisomeric anti-benzo[a]pyrene diol epoxide-deoxyguanosine adducts using phenyl liquid chromatography with diode array, fluorescence and tandem mass spectrometry detection. J. Chromatogr. A 1183, 119–128.

Fernandes, A., Liu, T., Amin, S., Geacintov, N.E., Grollman, A.P., Moriya, M., 1998. Mutagenic potential of stereoisomeric bay region (+)- and (−)-cis-anti-benzo[a]pyrene diol epoxide-N2-2′-deoxyguanosine adducts in *Escherichia coli* and simian kidney cells. Biochemistry (Mosc.) 37, 10164–10172.

Gammon, M.D., Sagiv, S.K., Eng, S.M., Shantakumar, S., Gaudet, M.M., Teitelbaum, S.L., Britton, J.A., Terry, M.B., Wang, L.W., Wang, Q., Stellman, S.D., Beyea, J., Hatch, M., Kabat, G.C., Wolff, M.S., Levin, B., Neugut, A.I., Santella, R.M., 2004. Polycyclic aromatic hydrocarbon-DNA adducts and breast cancer: a pooled analysis. Arch. Environ. Health 59, 640–649.

Gasiewicz, T.A., Kende, A.S., Rucci, G., Whitney, B., Willey, J.J., 1996. Analysis of structural requirements for Ah receptor antagonist activity: ellipticines, flavones, and related compounds. Biochem. Pharmacol. 52, 1787–1803.

Geacintov, N.E., Cosman, M., Hingerty, B.E., Amin, S., Broyde, S., Patel, D.J., 1997. NMR solution structures of stereoisometric covalent polycyclic aromatic carcinogen-DNA adduct: principles, patterns, and diversity. Chem. Res. Toxicol. 10, 111–146.

Grollman, A.P., Shibutani, S., 1994. Mutagenic specificity of chemical carcinogens as determined by studies of single DNA adducts. IARC Sci. Publ., 385–397.

Hecht, S.S., 2002. Tobacco smoke carcinogens and breast cancer. Environ. Mol. Mutagen. 39, 119–126.

Henry, E.C., Kende, A.S., Rucci, G., Totleben, M.J., Willey, J.J., Dertinger, S.D., Pollenz, R.S., Jones, J.P., Gasiewicz, T.A., 1999. Flavone antagonists bind competitively with 2,3,7, 8-tetrachlorodibenzo-p-dioxin (TCDD) to the aryl hydrocarbon receptor but inhibit nuclear uptake and transformation. Mol. Pharmacol. 55, 716–725.

Huang, X., Kolbanovskiy, A., Wu, X., Zhang, Y., Wang, Z., Zhuang, P., Amin, S., Geacintov, N.E., 2003. Effects of base sequence context on translesion synthesis past a bulky (+)-trans-anti-B[a]P-N2-dG lesion catalyzed by the Y-family polymerase pol kappa. Biochemistry (Mosc.) 42, 2456–2466.

Kapitulnik, J., Levin, W., Conney, A.H., Yagi, H., Jerina, D.M., 1977. Benzo[a]pyrene 7,8-dihydrodiol is more carcinogenic than benzo[a]pyrene in newborn mice. Nature 266, 378–380.

Kapitulnik, J., Wislocki, P.G., Levin, W., Yagi, H., Jerina, D.M., Conney, A.H., 1978. Tumorigenicity studies with diol-epoxides of benzo(a)pyrene which indicate that (±)-trans-7beta,8alpha-dihydroxy-9alpha,10alpha-epoxy-7,8,9,10-tetrahydrobenzo(a)pyrene is an ultimate carcinogen in newborn mice. Cancer Res. 38, 354–358.

Khan, A.U., Gilani, A.H., 2006. Selective bronchodilatory effect of Rooibos tea (*Aspalathus linearis*) and its flavonoid, chrysoeriol. Eur. J. Nutr. 45, 463–469.

Lee, J.E., Safe, S., 2000. 3′,4′-Dimethoxyflavone as an aryl hydrocarbon receptor antagonist in human breast cancer cells. Toxicol. Sci. 58, 235–242.

Levin, W., Wood, A.W., Chang, R.L., Slaga, T.J., Yagi, H., Jerina, D.M., Conney, A.H., 1977. Marked differences in the tumor-initiating activity of optically pure (+)- and (−)-trans-7,8-dihydroxy-7,8-dihydrobenzo(a)pyrene on mouse skin. Cancer Res. 37, 2721–2725.

Lin, L.Z., Lu, S., Harnly, J.M., 2007. Detection and quantification of glycosylated flavonoid malonates in celery, Chinese celery, and celery seed by LC-DAD-ESI/MS. J. Agric. Food Chem. 55, 1321–1326.

Lu, Y.F., Santostefano, M., Cunningham, B.D., Threadgill, M.D., Safe, S., 1995. Identification of 3′-methoxy-4′-nitroflavone as a pure aryl hydrocarbon (Ah) receptor antagonist and evidence for more than one form of the nuclear Ah receptor in MCF-7 human breast cancer cells. Arch. Biochem. Biophys. 316, 470–477.

Nebert, D.W., Dalton, T.P., Okey, A.B., Gonzalez, F.J., 2004. Role of aryl hydrocarbon receptor-mediated induction of the CYP1 enzymes in environmental toxicity and cancer. J. Biol. Chem. 279, 23847–23850.

Nebert, D.W., Roe, A.L., Dieter, M.Z., Solis, W.A., Yang, Y., Dalton, T.P., 2000. Role of the aromatic hydrocarbon receptor and [Ah] gene battery in the oxidative stress response, cell cycle control, and apoptosis. Biochem. Pharmacol. 59, 65–85.

Ohura, T., Morita, M., Kuruto-Niwa, R., Amagai, T., Sakakibara, H., Shimoi, K., 2010. Differential action of chlorinated polycyclic aromatic hydrocarbons on aryl hydrocarbon receptor-mediated signaling in breast cancer cells. Environ. Toxicol. 25, 180–187.

Pelkonen, O., Nebert, D.W., 1982. Metabolism of polycyclic aromatic hydrocarbons: etiologic role in carcinogenesis. Pharmacol. Rev. 34, 189–222.

Ravanat, J.L., Douki, T., Duez, P., Gremaud, E., Herbert, K., Hofer, T., Lasserre, L., Saint-Pierre, C., Favier, A., Cadet, J., 2002. Cellular background level of 8-oxo-7,8-dihydro-2′-deoxyguanosine: an isotope based method to evaluate artefactual oxidation of DNA during its extraction and subsequent work-up. Carcinogenesis 23, 1911–1918.

Reiners Jr., J.J., Lee, J.Y., Clift, R.E., Dudley, D.T., Myrand, S.P., 1998. PD98059 is an equipotent antagonist of the aryl hydrocarbon receptor and inhibitor of mitogen-activated protein kinase. Mol. Pharmacol. 53, 438–445.

Roberts-Thomson, S.J., McManus, M.E., Tukey, R.H., Gonzalez, F.F., Holder, G.M., 1993. The catalytic activity of four expressed human cytochrome P450s towards benzo[a]pyrene and the isomers of its proximate carcinogen. Biochem. Biophys. Res. Commun. 192, 1373–1379.

Ruan, Q., Gelhaus, S.L., Penning, T.M., Harvey, R.G., Blair, I.A., 2007. Aldo-keto reductase- and cytochrome P450-dependent formation of benzo[a]pyrene-derived DNA adducts in human bronchoalveolar cells. Chem. Res. Toxicol. 20, 424–431.

Shimada, T., 2006. Xenobiotic-metabolizing enzymes involved in activation and detoxification of carcinogenic polycyclic aromatic hydrocarbons. Drug Metab. Pharmacokinet. 21, 257–276.

Shimada, T., Oda, Y., Gillam, E.M., Guengerich, F.P., Inoue, K., 2001. Metabolic activation of polycyclic aromatic hydrocarbons and other procarcinogens by cytochromes P450 1A1 and P450 1B1 allelic variants and other human cytochromes P450 in *Salmonella typhimurium* NM2009. Drug Metab. Dispos. 29, 1176–1182.

Singh, R., Gaskell, M., Le Pla, R.C., Kaur, B., Azim-Araghi, A., Roach, J., Koukouves, G., Souliotis, V.L., Kyrtopoulos, S.A., Farmer, P.B., 2006. Detection and quantitation of benzo[a]pyrene-derived DNA adducts in mouse liver by liquid chromatography–tandem mass spectrometry: comparison with ^{32}P-postlabeling. Chem. Res. Toxicol. 19, 868–878.

Snijman, P.W., Swanevelder, S., Joubert, E., Green, I.R., Gelderblom, W.C., 2007. The antimutagenic activity of the major flavonoids of Rooibos (*Aspalathus linearis*): some dose–response effects on mutagen activation-flavonoid interactions. Mutat. Res. 631, 111–123.

Sundberg, K., Dreij, K., Seidel, A., Jernstrom, B., 2002. Glutathione conjugation and DNA adduct formation of dibenzo[a,l]pyrene and benzo[a]pyrene diol epoxides in V79 cells stably expressing different human glutathione transferases. Chem. Res. Toxicol. 15, 170–179.

Suzuki, N., Ohashi, E., Kolbanovskiy, A., Geacintov, N.E., Grollman, A.P., Ohmori, H., Shibutani, S., 2002. Translesion synthesis by human DNA polymerase kappa on a DNA template containing a single stereoisomer of dG-(+)- or dG-(−)-anti-N(2)-BPDE (7,8-dihydroxy-anti-9,10-epoxy-7,8,9,10-tetrahydrobenzo[a]pyrene). Biochemistry (Mosc.) 41, 6100–6106.

Takemura, H., Uchiyama, H., Ohura, T., Sakakibara, H., Kuruto, R., Amagai, T., Shimoi, K., 2010. A methoxyflavonoid, chrysoeriol, selectively inhibits the formation of a carcinogenic estrogen metabolite in MCF-7 breast cancer cells. J. Steroid Biochem. Mol. Biol. 118, 70–76.

Terashima, I., Suzuki, N., Shibutani, S., 2002. ^{32}P-Postlabeling/polyacrylamide gel electrophoresis analysis: application to the detection of DNA adducts. Chem. Res. Toxicol. 15, 305–311.

Whitlock Jr., J.P., 1999. Induction of cytochrome P4501A1. Annu. Rev. Pharmacol. Toxicol. 39, 103–125.

Williams, J.A., Phillips, D.H., 2000. Mammary expression of xenobiotic metabolizing enzymes and their potential role in breast cancer. Cancer Res. 60, 4667–4677.

THE JOURNAL OF BIOLOGICAL CHEMISTRY VOL. 285, NO. 20, pp. 15302–15313, May 14, 2010

Lipid Peroxidation Generates Body Odor Component *trans*-2-Nonenal Covalently Bound to Protein *in Vivo*[*][S]

Received for publication, September 22, 2009, and in revised form, March 7, 2010 Published, JBC Papers in Press, March 8, 2010, DOI 10.1074/jbc.M109.068023

Kousuke Ishino[‡], Chika Wakita[‡], Takahiro Shibata[‡], Shinya Toyokuni[§], Sachiko Machida[¶], Shun Matsuda[‖], Tomonari Matsuda[‖], and Koji Uchida[‡1]

From the [‡]Graduate School of Bioagricultural Sciences, Nagoya University, Nagoya 464-8601, the [§]Department of Pathology and Biological Responses, Graduate School of Medicine, Nagoya University, Nagoya 466-8550, the [¶]National Food Research Institute, 2-1-12 Kannondai, Tsukuba, Ibaraki 305-8642, and the [‖]Research Center for Environmental Quality Management, Kyoto University, 1-2 Otsu, 520-0811, Japan

***trans*-2-Nonenal is an unsaturated aldehyde with an unpleasant greasy and grassy odor endogenously generated during the peroxidation of polyunsaturated fatty acids. 2-Nonenal covalently modified human serum albumin through a reaction in which the aldehyde preferentially reacted with the lysine residues. Modified proteins were immunogenic, and a specific monoclonal antibody (mAb) 27Q4 that cross-reacted with the protein covalently modified with 2-nonenal was raised from mouse. To verify the presence of the protein-bound 2-nonenal *in vivo*, the mAb 27Q4 against the 2-nonenal-modified keyhole limpet hemocyanin was raised. It was found that a novel 2-nonenal-lysine adduct, *cis*- and *trans*-N^{ϵ}-3-[(hept-1-enyl)-4-hexylpyridinium]lysine (HHP-lysine), constitutes an epitope of the antibody. The immunoreactive materials with mAb 27Q4 were detected in the kidney of rats exposed to ferric nitrilotriacetate, an iron chelate that induces free radical-mediated oxidative tissue damage. Using high performance liquid chromatography with on-line electrospray ionization tandem mass spectrometry, we also established a highly sensitive method for detection of the *cis*- and *trans*-HHP-lysine and confirmed that the 2-nonenal-lysine adducts were indeed formed during the lipid peroxidation-mediated modification of protein *in vitro* and *in vivo*. Furthermore, we examined the involvement of the scavenger receptor lectin-like oxidized low density lipoprotein receptor-1 in the recognition of 2-nonenal-modified proteins and established that the receptor recognized the HHP-lysine adducts as a ligand.**

Lipid peroxidation in tissue and in tissue fractions represents a degradative process, which is the consequence of the production and propagation of free radical reactions primarily involving membrane polyunsaturated fatty acids, and has been implicated in the pathogenesis of numerous diseases, including atherosclerosis, diabetes, cancer, and rheumatoid arthritis, as well as in drug-associated toxicity, postischemic reoxygenation injury, and aging (1). The peroxidative breakdown of polyunsaturated fatty acids has also been implicated in the pathogenesis of many types of liver injuries and especially in the hepatic damage induced by several toxic substances. The lipid peroxidation leads to the formation of a broad array of different products with diverse and powerful biological activities. Among them are a variety of different aldehydes (2). The primary products of lipid peroxidation, lipid hydroperoxides, can undergo carbon-carbon bond cleavage via alkoxyl radicals in the presence of transition metals giving rise to the formation of short-chain, unesterified aldehydes or a second class of aldehydes still esterified to the parent lipid. These reactive aldehydic intermediates readily form covalent adducts with cellular macromolecules, including protein, leading to the disruption of important cellular functions. The important agents that give rise to the modification of protein may be represented by α,β-unsaturated aldehydic intermediates, such as 2-alkenals, 4-hydroxy-2-alkenals, and 4-oxo-2-alkenals (3, 4).

2-Alkenals represent a group of highly reactive aldehydes containing two electrophilic reaction centers. A partially positive carbon 1 or 3 in such molecules can attack nucleophiles, such as protein. It has been suggested that these aldehydes primarily react with the sulfhydryl group of cysteine, the ϵ-amino group of lysine, and the imidazole group of histidine in the proteins (2, 3). Among the 2-alkenals, 2-nonenal (Fig. 1*A*) has a characteristically unpleasant greasy and grassy odor. It is also a major contributor to the unpleasant cardboard flavor in aged beer. It was previously shown that 2-nonenal could be formed through lipid peroxidation as a minor product in peroxide-mediated oxidation of high concentrations of linoleic acid hydroperoxide or from liver microsomes treated with ADP/iron *in vitro* (2). Toyokuni *et al.* (5) also reported the production of C2–C12 saturated and unsaturated aldehydes, including 2-nonenal, in the kidney of rats exposed to Fe^{3+}-NTA.[2] More

* This work was supported by a grant-in-aid for scientific research on innovative areas (research in a proposed research area), from the Ministry of Education, Culture, Sports, Science and Technology, Japan (to K. U.).

[S] The on-line version of this article (available at http://www.jbc.org) contains supplemental Figs. S1–S22.

[1] To whom correspondence should be addressed. Fax: 81-52-789-5741; E-mail: uchidak@agr.nagoya-u.ac.jp.

[2] The abbreviations used are: Fe^{3+}-NTA, ferric nitrilotriacetate; AcLDL, acetylated LDL; BSA, bovine serum albumin; DiD, 1,1′-dioctadecyl-3,3,3′,3′-tetramethylindodicarbocyanine perchlorate; ELISA, enzyme-linked immunosorbent assay; HHP-lysine, N^{ϵ}-3-[(hept-1-enyl)-4-hexylpyridinium]lysine; HMBC, ^{1}H-detected multiple-bond connectivity; KLH, keyhole limpet hemocyanin; LDL, low density lipoprotein; LOX-1, lectin-like oxidized LDL receptor; HSA, human serum albumin; LC/ESI/MS/MS, high performance liquid chromatography with on-line electrospray ionization tandem mass spectrometry; mAb, monoclonal antibody; MRM, multiple reaction monitoring; PBS, phosphate-buffered saline; HPLC, high pressure liquid chromatography; CFP, cyan fluorescent protein; CHO, Chinese hamster ovary; Fmoc, *N*-(9-fluorenyl)-methoxycarbonyl; HSA, human serum albumin.